

Computational Study of H₂O Adsorption, Hydrolysis, and Water Splitting on (ZnO)₃ Nanoclusters Deposited on Graphene and Graphene Oxides

Duwage C. Perera* and Jayendran C. Rasaiah*



Cite This: ACS Omega 2023, 8, 32185–32203



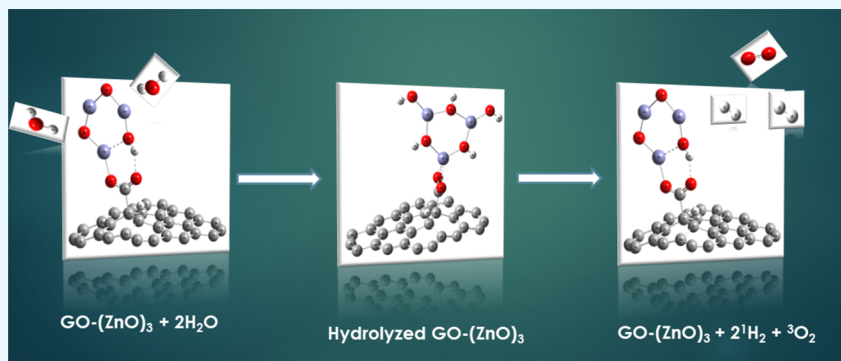
Read Online

ACCESS |

Metrics & More

Article Recommendations

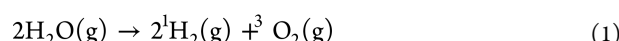
Supporting Information



ABSTRACT: Graphene and graphene oxide (GO)-based metal oxides could play an important role in using metal oxide like zinc oxide (ZnO) as photocatalysts to split water. The π conjugation structure of GO shows greater electron mobility and could enhance the photocatalytic performance of the bare ZnO catalyst by increasing the electron-hole separation. In this work, we use density functional theory (DFT) with the B3LYP exchange functional and DGDZVP2 basis set to study the impact of adsorbing (ZnO)₃ nanoparticles on graphene and four different GO models (GO1, GO2, GO4, and GO5) on the hydration and hydrolysis of water that precedes water splitting to produce H₂ and O₂ atoms in the gas phase and compare them with our previous studies on the bare catalyst in the absence of the substrate. The potential energy curves and activation energies are similar, but the triplet states are lower in energy than the singlet states in contrast to the bare (ZnO)₃ catalyst. We extend our calculations to water splitting from the hydrolyzed (ZnO)₃ on GO1 (GO1-(ZnO)₃). The triplet state energy remains lower than the singlet state energy, and hydrogen production precedes the formation of oxygen, but there is no energy inter-crossing during the formation of O₂ that occurs in the absence of a GO1 substrate. Although the hydrolysis reaction pathway follows similar steps in both the bare and GO1-(ZnO)₃, water splitting with (ZnO)₃ absorbed on the GO1 substrate skips two steps as it proceeds toward the production of the second H₂. The production of two hydrogen molecules precedes oxygen formation during water splitting, and the first Zn–H bond formation step is the rate-determining step. The ZnO trimer deposited on GO systems could be potentially attractive nanocatalysts for water splitting.

INTRODUCTION

Ever since Fujishima and Honda first discovered in 1972, the electrochemical photolysis of water in the presence of TiO₂ catalyst to produce H₂ gas has become an active research area to better understand the mechanism of photolysis, and find cheaper substitutes to TiO₂ as solutions to current energy problems.¹ Numerous studies show that other nanoscaled metal oxides can also play an important role as photocatalysts in water-splitting reactions 1 to produce H₂, overcoming the cost and other challenges of TiO₂.^{2–4} However, scaling up H₂ gas production using metal oxides or metal oxide co-catalysts derived from noble metals like Pt, Ru, and Rh is a problem due to the high temperatures required for synthesis and related costs. There is also the problem of finding suitable substrates for the photo-catalysts to operate at room temperature.⁵



We note that the oxygen and hydrogen atoms formed on water splitting are in their triplet and singlet states, respectively, that are also their most stable states at ambient temperatures. The enthalpy change for the reaction is 116.5 kcal/mol at 298.15 K in the gas phase showing that the reaction is strongly endothermic, and requires \approx two photons of 500 nm wavelength

Received: July 7, 2023

Accepted: July 25, 2023

Published: August 21, 2023



if the reaction occurs photochemically to overcome the enthalpy difference⁶ of reaction 1. However, on examining the mechanistic details of the reaction 1 using TiO₂ and different metal oxide catalysts, water splitting is preceded by hydration of the catalyst and hydrolysis of water. This lowers the enthalpies of the intermediates thereby increasing the enthalpy for water splitting even more than what is needed for the direct dissociation of two molecules of water to form two molecules of hydrogen (H₂) and one molecule of oxygen (O₂) according to the equation 1. It is important to study the precursors to water splitting as already done by Fang et al. for (TiO_n)_{n=1-4} and other metal oxides to get a clearer picture of the steps preceding water splitting in the gas phase, using metal oxide catalysts. We have previously studied the bare (ZnO)_{n=3} nanoparticle as a substitute for TiO₂ as a catalyst. The goal of this paper is to study the electronic properties of ZnO trimer deposited on graphene and various synthetic graphene oxides for possible use as a catalyst or photocatalyst for water splitting. Graphene shows excellent electron mobility due to its π conjugated structure,⁷ which should make it an appropriate substrate that can accept electrons for exciton separation. However, the hydrophobic property of graphene makes it unsuitable for water-splitting reactions. On the other hand, "suitably functionalized" graphene oxide(GOs) are hydrophilic and have tunable properties and multiple functions that can make them useful substrates as photocatalysts to split water. By "functionalized" we mean different chemical groups attached to graphene to form different GOs.⁸⁻¹¹ Certain metal oxide-decorated carbon materials including GO have also attracted researchers as they exhibit enhanced stability, durability, electrocatalytic, and photocatalytic properties.¹²⁻²⁴

Since TiO₂ is the most widely studied photocatalyst, systems combining GO and TiO₂ have become an important field of study that probe changes in photocatalytic efficiencies of different combinations of GO-TiO₂. The π electrons on suitable GOs can bond with Ti atoms in TiO₂ to fine-tune their window of light absorption. The GO-TiO₂ systems can also form a heterojunction between p-type GO and n-type TiO₂, which operates as a separator of photogenerated electron-hole pairs.²⁵⁻²⁷ In this paper, we report on our study of replacing GO-TiO₂ with GO1-(ZnO)₃ as a catalyst for splitting water.

ZnO is also a semiconductor with a wide band gap (about 3.37 eV at room temperature)²⁸ and a wide range of potential applications. ZnO nanoclusters are also known to be highly active photocatalysts and are commercially cheaper than TiO₂.²⁹ Similar to TiO₂, ZnO can also form a p-n heterojunction with a suitable GO for visible light absorption, that could be a better photocatalyst for water splitting³⁰⁻³³ than some others that are currently in use. Previous computational studies of ZnO(1010) and (1020) sheets in water using QM/MD or neural networks reveal spontaneous partial dissociation of water on the surfaces with proton transfer between adsorbed or bulk water to the surface oxygen atom of the ZnO layer.³⁴⁻³⁸ Motivated by these reports in the literature,⁶ and our own study of bare (ZnO)₃ nanoclusters,³⁹ our ultimate goal is to investigate the mechanism of H₂ and O₂ production via the water splitting reaction 1 using the same (ZnO)₃ nanoclusters but now deposited on graphene or suitably functionalized graphene oxides (GOs) anchored on graphene that could be better and cheaper than the TiO₂ catalyst. An essential step, prior to water splitting in the gas phase, is the adsorption of a water molecule on the zinc atom of the photocatalyst followed by hydrolysis that involves dissociation of the adsorbed water via proton transfer to a

neighboring oxygen atom on the ZnO ring. This hydrolytic process is repeated with the second water molecule and has been studied by us³⁹ recently using the bare ZnO trimer as a catalyst. There are no additional water molecules to solvate each (ZnO)₃ nanocluster as would occur if the lattices were exposed to several water layers or were immersed in an aqueous electrolyte. Following these two steps, the production of H₂ and O₂ occurs through water splitting even in the absence of light as found in calculations with the bare catalyst.^{6,39} It is the mechanisms of these reactions on graphene and on functionalized GOs that are studied in this paper, which are of importance in themselves, and also as a prelude to understanding what occurs when the system is solvated further with more water molecules beyond the bare stoichiometric minimum required 1, which is two water molecules for each ZnO trimer and also in the absence of light.

To implement the restricted case in the absence of light, we need to be specific about the computational method and the form of the catalyst. We use density functional theory (DFT) with the same basis set and exchange functional that was used in our earlier study of the catalytic activity of bare (ZnO)₃ nanoclusters.³⁹ As before, the triplet state was approximated as the singlet state of spin one S₁. We found that the energies of triplet states S₁ are lower than the energies of ground states of spin zero S₀ unlike the energy of the bare (ZnO)₃ nanoclusters.³⁹ We also calculate the energies of absorption and hydrolysis of H₂O on the ZnO trimers in the singlet and triplet states to understand the thermodynamics of adsorption and hydrolysis in each state and construct the corresponding potential energy surfaces (PES) to gain insight into the mechanism of the two processes, and the energy gaps between the singlet and triplet states at different stages of adsorption and hydrolysis. Following this we discuss the reaction pathways for the formation of hydrogen and oxygen on two of the zinc oxide nanocatalysts (ZnO)₃ deposited on graphene oxides, GO1, and compare them with what occurs with the bare catalyst that we studied earlier. To the best of our knowledge, this study of different combinations of (ZnO nanocluster-GO) systems has not been reported in the literature.

COMPUTATIONAL METHOD AND SYSTEM SETUP

We first studied how (ZnO)₃ is absorbed on the graphene sheet in both the parallel and vertical directions to the surface, followed by a study of adsorption and hydrolysis on five GO models deposited on graphene. Since determining the exact structure of synthetic GOs is difficult, we modeled the GO surfaces by adding functionality to the optimized graphene sheet using carboxyl, hydroxyl, and epoxy groups similar to the study by Huang and Gubbins.⁴⁰ Even though the structures of GO models have still debated the high-resolution solid-state,¹³ C NMR studies show the existence and the positions of hydroxyl, epoxy, and sp² C components on GO surfaces.^{41,42} The graphene sheet was constructed with periodic boundary conditions (PBC) as explained in the Gaussian tutorial using a benzene ring⁴³ as a replication unit. A graphene layer of 30 C atoms is numbered as shown in Figure 1 to make it easier to follow our constructions and description of the GO models. We introduced the required functional groups at C atoms 21, 10, 8, and 11 to make different GO models. We then adsorbed (ZnO)₃ on the graphene sheet and separately on the functional groups of the GO model systems already attached to the graphene sheets. The optimized (ZnO)₃ is shown in the Figure 2, and the Zn and O atoms are also numbered to characterize charges, bonds, bond lengths, and details of the reaction pathway.

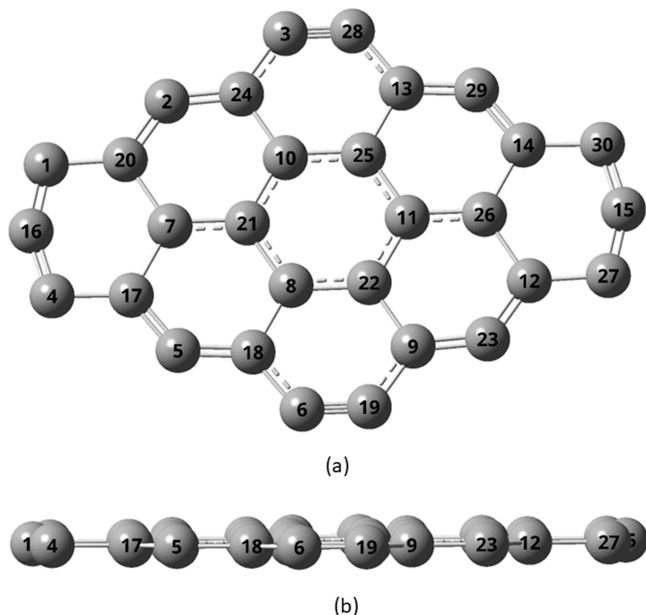


Figure 1. Optimized graphene layer using B3LYP/DGDZVP2 (a) top view and (b) side view. C atoms are represented in grey color.

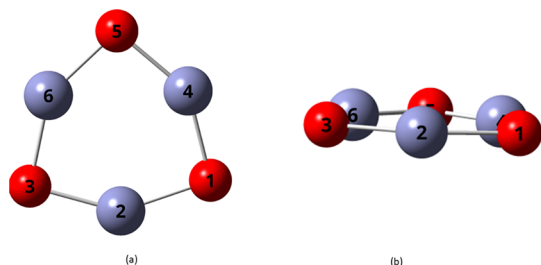


Figure 2. Optimized singlet state ZnO trimer using B3LYP/DGDZVP2. (a) Top view and (b) side view. Zn and O atoms are represented using light blue and red colors, respectively. The numbers identify specific Zn and O atoms.

Table 1. Selected GO Models with $-COOH$, $-OH$, and Epoxy Functional Groups^a

C atom attached to the functional group	GO model				
	GO1	GO2	GO3	GO4	GO5
C21	$-COOH$	$-COOH$	$-OH$	$-COOH$	O
C8	H				O
C11	H	H		$-OH$	

^aThe C atoms in the GO5 model are the atoms C21 and C8 on which the epoxy group is formed. The C atom is numbered as shown in Figure 1.

All the above structures were optimized using the Becke–Lee–Yang–Parr (B3LYP) exchange-correlation functional and DGDZVP2 Dunning basis set using DFT.^{44,45} The calculation method and specific ZnO cluster system were chosen based on our previous benchmark and basis set studies of small ZnO nanoclusters comparing $(ZnO)_n$, where $n = 1–6$.³⁹ We recall that the exchange functional/basis set combination was chosen by us as the best of 30 such combinations of exchange functionals and basis sets, and the optimal size of the $(ZnO)_n$ was chosen as $n = 3$ for the best match energy singlet–triplet energy gap with $n = 6$ as an alternative. Here, the triplet state is

considered as the singlet state with multiplicity $2S + 1 = 3$ as in our previous calculations. The energy gaps for $n = 3$ and $n = 6$ are closer to 57.8 kcal/mol, which is the energy of two visible photons at the 500 nm wavelength, required to split two water molecules to produce $2H_2$ and O_2 .³⁹ We used only the $n = 3$ nanocluster instead of using both $n = 3$ and 6, considering the $n = 3$ system would be computationally less complex and less expensive model systems. We calculated the binding energy of $(ZnO)_3$ on graphene and on the functional groups of each GO model using the same level of theory considering the complexity and the computational time that would be required for $n = 6$ nanoclusters. We also calculated and compared the geometric properties and the free energy and enthalpy changes that accompanied $(ZnO)_3$ adsorption. To each optimized graphene– $(ZnO)_3$ and GO– $(ZnO)_3$ model, we introduced one water molecule to study not only the corresponding binding energy but other properties such as Mulliken charges and changes in the bond length of atoms in $(ZnO)_3$. The hydration and hydrolysis reaction on the selected systems was continued using the second water molecule. We used the hydrolyzed products of the GO1– $(ZnO)_3$ to study the reaction pathway of H_2 and O_2 production.

The same calculation steps were studied on both the singlet (ground state) and triplet states (modeled as the excited state of the singlet state with $S = 1$, to overcome the calculation complexity of studying an excited state using DFT). This provides information on the reorganization and redistribution of charge on the absorbed water molecules before splitting occurs.

All geometry optimization and structural and electronic property calculations were carried out using Gaussian 16 software package⁴⁶ and GaussView 6 graphical interface implemented on the University of Maine High-Performance Computer (HPC) resources.

Optimized Graphene and Graphene Oxide Models. In this section, we present the results of our studies of graphene and five different GO models chosen as substrates for the ZnO photocatalyst. The top and side views of the optimized singlet state graphene structures are shown in Figure 1. The GO models are obtained by attaching carboxyl, hydroxyl, and epoxy functional groups to the graphene layer, as shown in Table 1. The C atom numbering is shown in Figure 1. The optimized ground-state GO models are shown in Figure 3, and the triplet state structures are displayed in the SI document. When a functional group is attached to a carbon atom (chosen as C21) in the graphene sheet in GO models 1–3, the electrons on the neighboring carbon atoms are unpaired to form a double-bond, the (π conjugated system) breaks, and the unpaired carbon atoms become saturated with hydrogen atoms. The optimized energies and geometric properties of the GO models in both the singlet and triplet states are tabulated in the SI document.

In GO1, GO2, and GO4 models, the functional group $-COOH$ is attached to the C21 atom of graphene with an additional H atom attached to C8 for GO1, and to C11 for GO2. GO4 is similar to GO2 except that an $-OH$ group replaces H at C11 and GO3 is similar to GO2 except that an OH group replaces the $-COOH$ group at C21. In the GO5 model, the functional epoxy O atom straddles C21 and C8 atoms of graphene. All the GO models are twisted and inclined away from the planar graphene structure at the point of attachment to the functional in both ground and triplet states.

$(ZnO)_3$ Adsorption on Graphene and Graphene Oxides GO1–GO5. We next attached the optimized $(ZnO)_3$ to graphene and to each GO model before reoptimizing the composite system. The $(ZnO)_3$ cluster is bonded via the Zn2

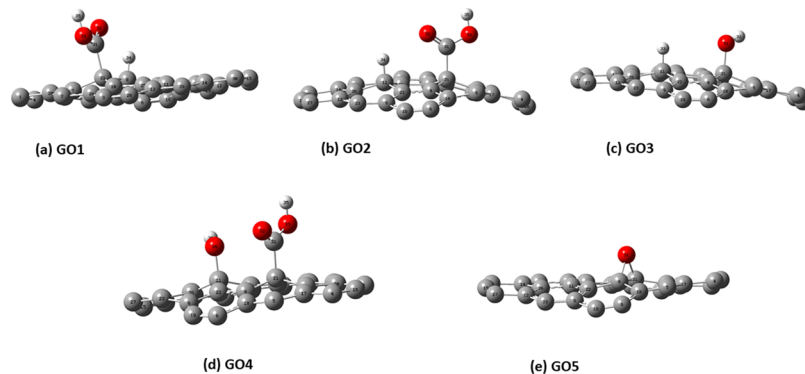


Figure 3. Optimized GO models, (a) GO1, (b) GO2, (c) GO3, (d) GO4, and (e) GO5 using B3LYP/DGDZVP2 level of theory. Grey, red, and light grey color schemes represent the C, O, and H atoms, respectively. The top views of all the GO models are in the [SI](#) document.

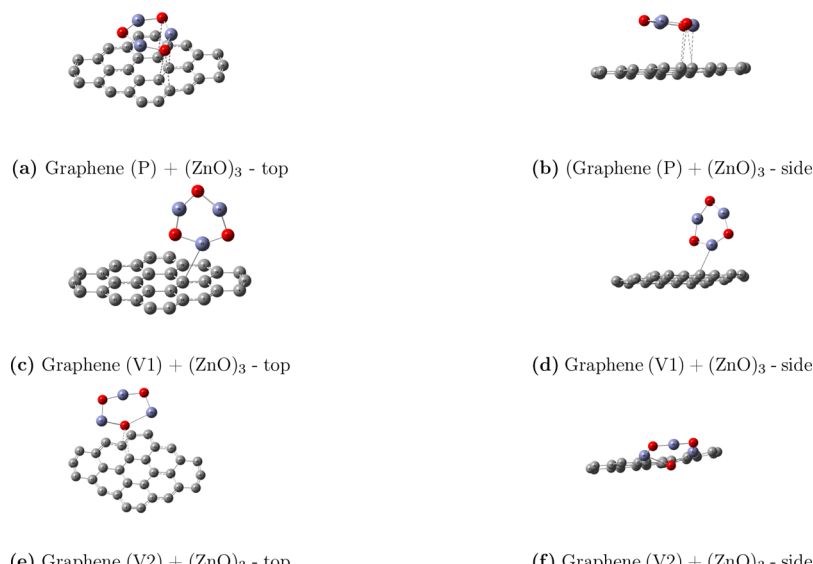


Figure 4. Optimized structures of ZnO trimer adsorbed on graphene in the singlet state. (a) Top view of $(\text{ZnO})_3$ absorbed parallel to the graphene, (b) side view of $(\text{ZnO})_3$ absorbed parallel to the graphene, (c) top view of $(\text{ZnO})_3$ absorbed vertically through a Zn atom to the C atom on graphene, (d) side view of $(\text{ZnO})_3$ absorbed vertically through a Zn atom to a C atom on graphene, (e) top view of $(\text{ZnO})_3$ absorbed vertically through a O atom to two C atoms on graphene, and (f) side view of $(\text{ZnO})_3$ absorbed vertically through O atom to the graphene using B3LYP/DGDZVP2 level of theory. The optimized triplet state structures are displayed in the SI document.

atom and/or adjacent O atom ([Figure 2](#)) to graphene in three ways in parallel and vertical configurations. The optimized structures in the singlet state are displayed in [Figure 4](#), and the triplet state structures are in the [SI](#) document. The vertical adsorption of $(\text{ZnO})_3$ on graphene occurs by forming a Zn–C bond or two O–C bonds. The parallel structure is obtained by an adjacent pair of Zn and O atoms on $(\text{ZnO})_3$ bonding to a pair of C atoms on graphene. [Figure 5](#) shows the optimized $(\text{ZnO})_3$ on GO models in the singlet state. The triplet state structures are shown in the [SI](#) document.

We now discuss the adsorption and bonding of $(\text{ZnO})_3$ in the GO models. Figure 5 shows the optimized $(\text{ZnO})_3$ in the GO models in their respective singlet states. As seen in the figure, $(\text{ZnO})_3$ makes a strong bond with the O atom of the carboxyl group in all GO1, GO2, and GO4 models via a Zn atom. In GO3, the bonding is between the Zn atom and C atom of the graphene sheet, and in GO5, the bonding is between a Zn atom and the O atom that straddles two C atoms on the graphene sheet—see Table 1. The triplet state structures are displayed in the SI document. We do not consider the GO3 model further to save space without detracting from our main conclusions.

$(\text{ZnO})_3$ adsorption energies on graphene and GO models are of interest with respect to their stability as catalytic sites and were calculated using eqs 2 and 3 in kcal/mol, respectively, with the results displayed in the Table 2 along with the free energy and enthalpy of adsorption.

$$E_{\text{Adl}} = E_{\text{Tot}} - (E_{\text{ZnO}_x} + E_{\text{Graphene}}) \quad (2)$$

$$E_{\text{Ad2}} = E_{\text{Tot}} - (E_{\text{ZnO}_x} + E_{\text{GO}}) \quad (3)$$

In eq 2, E_{Tot} is the energy of the system after adsorbing $(\text{ZnO})_3$ on graphene, and in eq 3, it is the energy of the system after adsorbing $(\text{ZnO})_3$ on a GO model. The energy and free energy of adsorption at 300 K are more negative in the triplet than in the singlet states, and more negative for the GO models than for graphene, which is reflected in the more negative total energies of the triple states than the singlet states. Adsorption is driven by a negative enthalpy change and a small positive entropy change possibly due to the rotational entropy of the ZnO trimer. Adsorption of the ZnO trimer parallel to graphene is less favorable in the singlet state than in the triplet state. The magnitudes of the energy and free energy of adsorption (-50

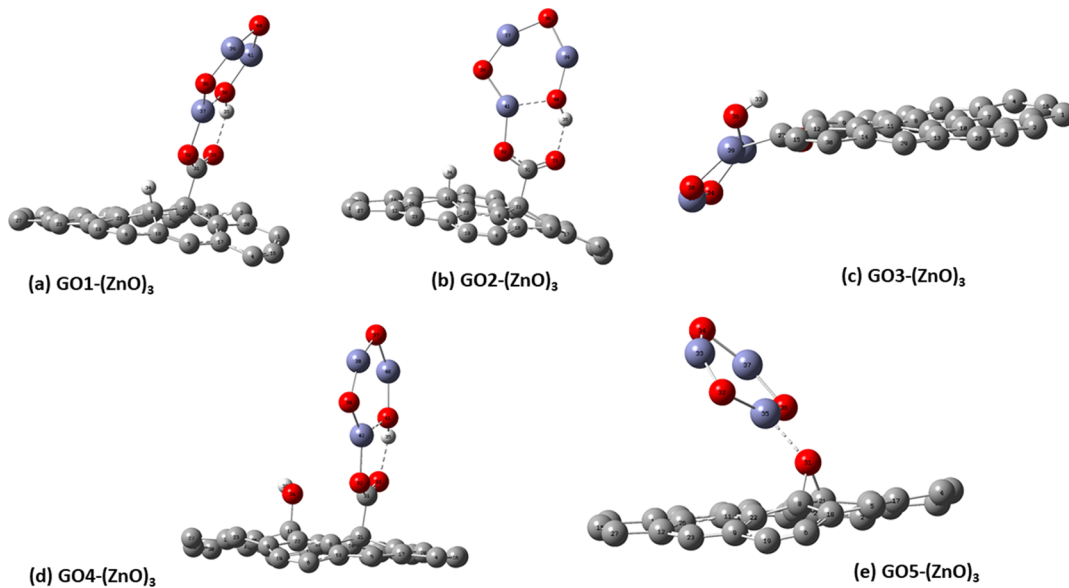


Figure 5. Optimized structures of $(\text{ZnO})_3$ absorbed on (a) GO1, (b) GO2, (c) GO3, (d) GO4, and (e) GO5, respectively, in the singlet state using B3LYP/DGDZVP2 level of theory. See the SI document for the corresponding triplet state structures.

Table 2. Energies, Free Energies ΔG , and Enthalpies ΔH of Adsorption of $(\text{ZnO})_3$ Cluster on Graphene and GO Models at 300 K

system B3LYP/DGDZVP2	E_{Ad} in kcal/mol		ΔG in kcal/mol		ΔH in kcal/mol	
	singlet	triplet	singlet	triplet	singlet	triplet
$(\text{ZnO})_3$ -graphene-vertical 1	-6.40	-89.09	-12.39	-93.83	-6.02	-86.74
$(\text{ZnO})_3$ -graphene-vertical 2	-142.68		-138.94		-139.10	
$(\text{ZnO})_3$ -graphene-parallel	-3.04	-257.70	-8.25	-251.90	-3.29	-251.21
$(\text{ZnO})_3$ -GO1	-50.46	-108.35	-53.92	-111.87	-49.68	-107.26
$(\text{ZnO})_3$ -GO2	-49.86	-108.01	-53.75	-111.85	-49.21	-106.74
$(\text{ZnO})_3$ -GO4	-51.78	-108.28	-55.33	-111.56	-51.10	-107.06
$(\text{ZnO})_3$ -GO5	-12.83	-100.55	-17.12	-101.89	-11.65	-97.08

Table 3. Bond Lengths between Atoms on $(\text{ZnO})_3$ Before and After Absorption on Graphene and GO Systems^a

model	bond length in Å					
	4Zn–1O	2Zn–3O	6Zn–3O	6Zn–5O	4Zn–5O	2Zn–1O
$(\text{ZnO})_3$	1.833(1.950)	1.833(1.950)	1.833(1.833)	1.833(1.829)	1.833(1.829)	1.833(1.833)
$(\text{ZnO})_3$ -graphene-vertical 1	1.847(1.851)	1.859(1.851)	1.825(1.824)	1.829(1.832)	1.834(1.832)	1.823(1.824)
$(\text{ZnO})_3$ -graphene-parallel	1.833	1.833	1.834	1.833	1.836	1.835
$(\text{ZnO})_3$ -GO1	1.834(1.836)	2.073(2.096)	1.837(1.831)	1.802(1.803)	1.840(1.840)	1.795(1.792)
$(\text{ZnO})_3$ -GO2	1.836(1.838)	2.074(2.087)	1.835(1.831)	1.802(1.803)	1.839(1.840)	1.794(1.792)
$(\text{ZnO})_3$ -GO4	1.832(1.837)	2.085(2.098)	1.833(1.829)	1.802(1.804)	1.840(1.840)	1.793(1.792)
$(\text{ZnO})_3$ -GO5	1.857(1.876)	1.870(1.868)	1.818(1.811)	1.830(1.834)	1.832(1.830)	1.818(1.813)

^aTriplet state lengths are shown in parenthesis.

kcal/mol), for the GO models except for GO5, and graphene (vertical1 and parallel) in the singlet states, suggest chemical bonding rather than physical adsorption—see Table 2. The energy of adsorption of the ZnO trimer on GO5 (-12.83 kcal/mol) in the singlet state is less negative for the other GO models. Interestingly, the triplet structures have lower energies (-100 kcal/mol) of adsorption than the corresponding singlet states, unlike the bare ZnO trimer where the order is reversed.³⁹

The adsorption of the $(\text{ZnO})_3$ on graphene and on GO models is accompanied by charge distribution on the atoms and changes in bond lengths between atoms of the ZnO nanocluster. The bond lengths between the Zn and O atoms in the $(\text{ZnO})_3$ nanocluster and between the nanocluster and the atoms in the graphene and GO models were calculated using DFT with the

B3LYP/DGDZVP2 exchange functional and basis set. The bond lengths between the atoms on $(\text{ZnO})_3$ are shown in Table 3.

In the bare $(\text{ZnO})_3$ nanocluster, the Zn–O bond length is 1.833 \AA in the singlet state. All the triplet state bond lengths are greater or nearly the same as the singlet state values. The Zn–O bond lengths in the trimer are not changed significantly when $(\text{ZnO})_3$ is adsorbed parallel to graphene. The bond lengths 4Zn–1O, 4Zn–5O, and 6Zn–3O of the trimer in the singlet state are increased when binding vertically to the graphene sheet and to the GO models via the 2Zn atom. The 2Zn–3O bond length is increased while the 2Zn–1O and 6Zn–5O bond lengths are decreased. The numbering of the Zn and oxygen atoms of the ZnO trimer are shown in Figure 2.

Table 4. Bond Lengths between Atoms on $(\text{ZnO})_3$ and Atoms on Graphene or GO Systems in the Singlet and Triplet States after Adsorption

model	bond length in Å		
	bond	singlet	triplet
$(\text{ZnO})_3\text{-GV1}$	2Zn-C	2.954	2.741
$(\text{ZnO})_3\text{-GV2}$	SO-C	2.369	N/A
$(\text{ZnO})_3\text{-GP}$	4Zn-C	3.302	N/A
	SO-C	3.409	N/A
$(\text{ZnO})_3\text{-GO1}$	2Zn-O	1.923	1.908
	3O-H	0.984	0.988
$(\text{ZnO})_3\text{-GO2}$	2Zn-O	1.917	1.909
	3O-H	0.985	0.990
$(\text{ZnO})_3\text{-GO4}$	2Zn-O	1.915	1.907
	3O-H	0.983	0.991
$(\text{ZnO})_3\text{-GO5}$	2Zn-O	2.183	2.152

The bond lengths between atoms on $(\text{ZnO})_3$ and selected atoms on graphene or GO systems in the singlet and triplet states are displayed in the Table 4.

The 2Zn-C(graphene) and 2Zn-O(GO) bond lengths in the triplet state are shorter than the corresponding singlet state bond lengths. This signals the appearance of stronger bonds in the triplet state with lower optimized energies compared to the singlet state. However, the 3O($(\text{ZnO})_3$)-H(GO) bond lengths are larger in the triplet state than in the singlet state corresponding to weaker bonds in the triplet states. Overall there is a correlation between the bond type, bond lengths, and adsorption energies of the ZnO trimer.

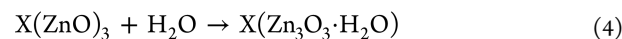
We next consider the adsorption of a water molecule on the ZnO trimer just before hydrolysis. The Mulliken charges on atoms of the $(\text{ZnO})_3$ cluster before and after adsorption of water on graphene and graphene oxide shown in the Table 5 were calculated using the same DFT and exchange functional and basis set. Although not unique, the Mulliken charges on the atoms provide a qualitative understanding of the changes in

charge density before and after the absorption of a water molecule on graphene and GO models. The zinc atoms are positively charged, and the oxygen atoms are negatively charged. When a water molecule is absorbed, the oxygen atom of water with a residual negative charge is attached to one of the three positively charged Zn atoms of the ZnO trimer.

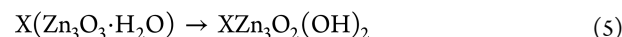
Polarization follows from a small rearrangement of charge. For the bare ZnO trimer, the partial positive charge on the 2Zn atom, which is the binding site, is increased slightly while the magnitude of the negative charge of the adjacent 1O atom is also increased, and less so for the other oxygen atoms (3O and SO) on the ring. Similar considerations apply when the ZnO is adsorbed on a substrate as in graphene or the GO models. Now there are two charge rearrangements, one accompanying bonding with the substrate and the other following adsorption of a water molecule before hydrolysis which depends on the respective binding sites. The charge on 2Zn of GO5 structure decreases after water adsorption accompanied by a larger decrease in the negative charge of the 1O oxygen atom in GO5 than in other systems. This could be a reflection of the epoxy structure of GO5. Likewise, the densities of state and band gaps provide information on how electron excitation of the $(\text{ZnO})_3$ catalytic center is modulated by graphene and GO model substrates. Our calculations using the B3LYP/DGDZVP2 level of DFT theory are displayed in Figure 6. As seen in Figure 6, the HOMO-LUMO gap, E_g is smaller in the GO models compared to the bare ZnO trimer.

RESULTS AND DISCUSSION

We next discuss successive steps of adsorption and hydrolysis of two water molecules that occur prior to water splitting.³⁹ The first adsorption step



is followed by hydrolysis

**Table 5. Mulliken Charges of Atoms in $(\text{ZnO})_3$ without and with H_2O before and after Adsorb on the Graphene and GO Models in the Singlet State^a**

system B3LYP/DGDZVP2	Mulliken charges					
	1O	2Zn	3O	4Zn	5O	6Zn
$(\text{ZnO})_3$	-0.757	0.757	-0.757	0.757	-0.757	0.757
$(\text{ZnO})_3 + \text{H}_2\text{O}$	-0.886	0.779	-0.764	0.738	-0.778	0.750
$(\text{ZnO})_3\text{-graphene-parallel}$	-0.745	0.736	-0.744	0.746	-0.741	0.747
$(\text{ZnO})_3\text{-graphene-vertical}$	-0.767	0.665	-0.811	0.758	-0.753	0.766
$(\text{ZnO})_3\text{-graphene + H}_2\text{O-vertical 1-pathway 1}$	-0.776	0.702	-0.912	0.759	-0.773	0.752
$(\text{ZnO})_3\text{-graphene + H}_2\text{O-vertical 1-pathway 2}$	-0.766	0.680	-0.828	0.783	-0.878	0.753
$(\text{ZnO})_3\text{-GO1}$	-0.753	0.786	-0.715	0.767	-0.724	0.835
$(\text{ZnO})_3\text{-GO1 + H}_2\text{O-pathway 1}$	-0.876	0.815	-0.701	0.743	-0.745	0.814
$(\text{ZnO})_3\text{-GO1 + H}_2\text{O-pathway 2}$	-0.768	0.775	-0.737	0.767	-0.779	0.801
$(\text{ZnO})_3\text{-GO2}$	-0.725	0.767	-0.759	0.829	-0.711	0.774
$(\text{ZnO})_3\text{-GO2 + H}_2\text{O-pathway 1}$	-0.746	0.745	-0.888	0.813	-0.698	0.807
$(\text{ZnO})_3\text{-GO2 + H}_2\text{O-pathway 2}$	-0.783	0.767	-0.773	0.797	-0.731	0.763
$(\text{ZnO})_3\text{-GO4}$	-0.726	0.766	-0.751	0.833	-0.721	0.780
$(\text{ZnO})_3\text{-GO4 + H}_2\text{O-pathway 1}$	-0.784	0.766	-0.764	0.800	-0.734	0.768
$(\text{ZnO})_3\text{-GO4 + H}_2\text{O-pathway 2}$	-0.746	0.744	-0.880	0.814	-0.704	0.809
$(\text{ZnO})_3\text{-GO5}$	-0.778	0.745	-0.755	0.711	-0.804	0.753
$(\text{ZnO})_3\text{-GO5 + H}_2\text{O-pathway 1}$	-0.901	0.738	-0.773	0.766	-0.820	0.755
$(\text{ZnO})_3\text{-GO5 + H}_2\text{O-pathway 2}$	-0.814	0.722	-0.808	0.721	-0.779	0.738

^aThe atoms are numbered as in Figure 2.

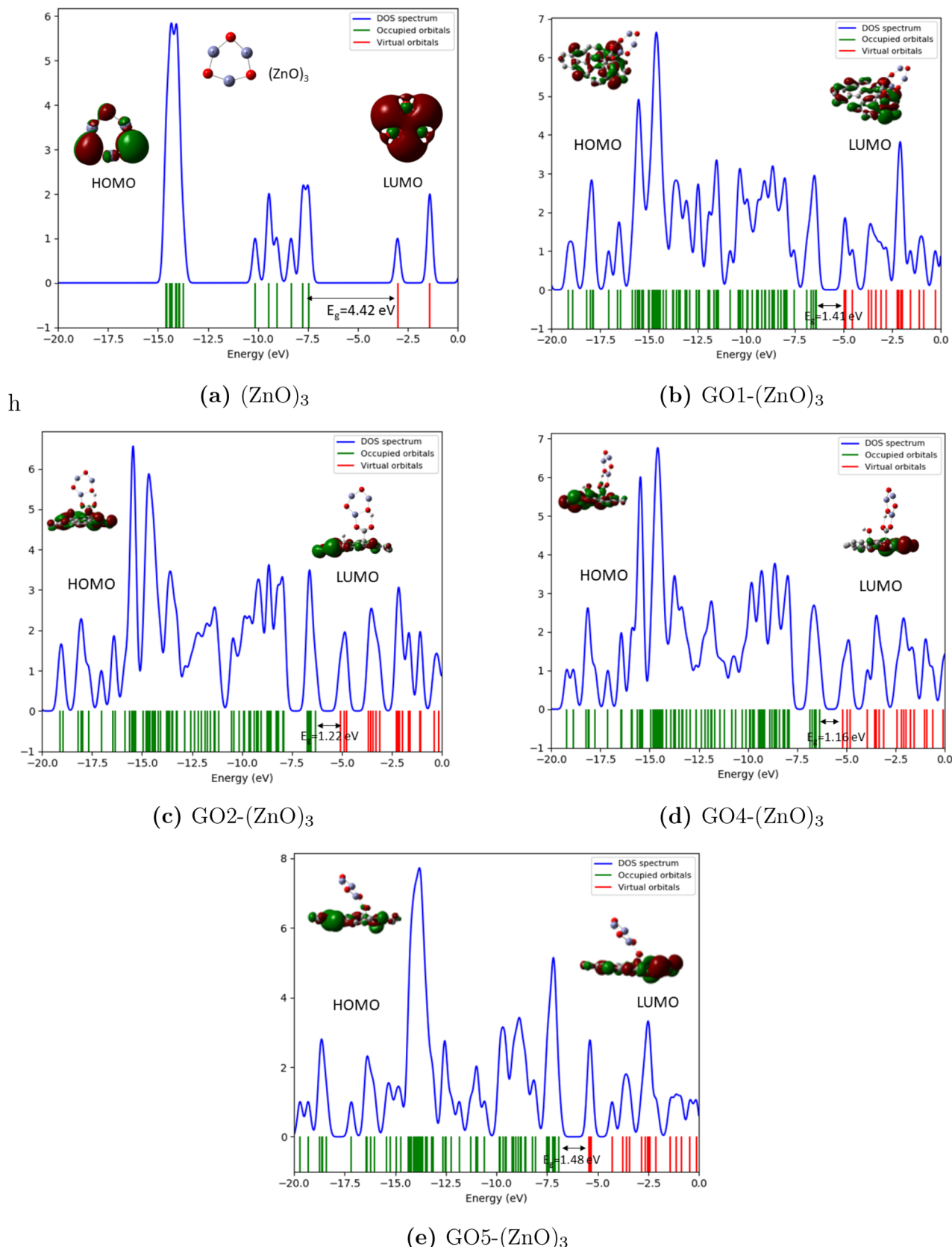


Figure 6. Calculated density of states using GaussSum for (a) $(\text{ZnO})_3$, and $(\text{ZnO})_3$ adsorbed on (b) GO model 1; GO1, (c) GO model 2; GO2, (d) GO model 4; GO4, and (e) GO model 5; GO5.

Likewise, the adsorption of the second water molecule



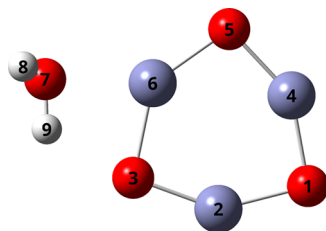
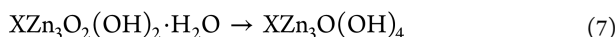


Figure 7. Optimized structures of H_2O adsorbed on $(\text{ZnO})_3$ using B3LYP/DGDZVP2 level of theory. Zn, O, and H atoms are represented using the blue, red, and grey colors, respectively.

is followed by hydrolysis



where X is either graphene or a GO system. If X is removed, what remains is the bare $(\text{ZnO})_3$ nanocluster and its hydrated and hydrolyzed products discussed in our earlier study.³⁹

H₂O Absorption on Catalytic Sites. The adsorption of a water molecule occurs directly on a Zn atom of the ZnO trimer already adsorbed on graphene or on the ZnO trimer bonded to a functional group in GO. This is of interest as it is the catalytic site at which hydrolysis begins before water splitting. The negatively charged oxygen atom of a water molecule is adsorbed onto a positively charged Zn atom of the ZnO trimer followed by hydrolytic dissociation and proton transfer of a hydrogen atom to an oxygen atom adjacent to zinc.

Figure 7 shows the adsorption of a water molecule on the bare $(\text{ZnO})_3$ catalyst in the singlet state. A detailed study on the adsorption and hydrolysis reaction of this system was described in our previous study.³⁹ In Figures 8 and 9, we follow the reaction of the first water molecules with $(\text{ZnO})_3$ deposited on graphene and GO models. Figure 8 displays water molecule adsorption on graphene-(ZnO)₃ model, where V1 and V2 represent two different vertical configurations of $(\text{ZnO})_3$ on graphene in the singlet state. After forming a Zn–O bond, two O atoms adjacent to the binding site have valence electrons poised to form a O–H bond with one of the two H atoms of the water molecule. Hence, both V1 and V2 arrangements can lead to two different hydrolysis reaction pathways.

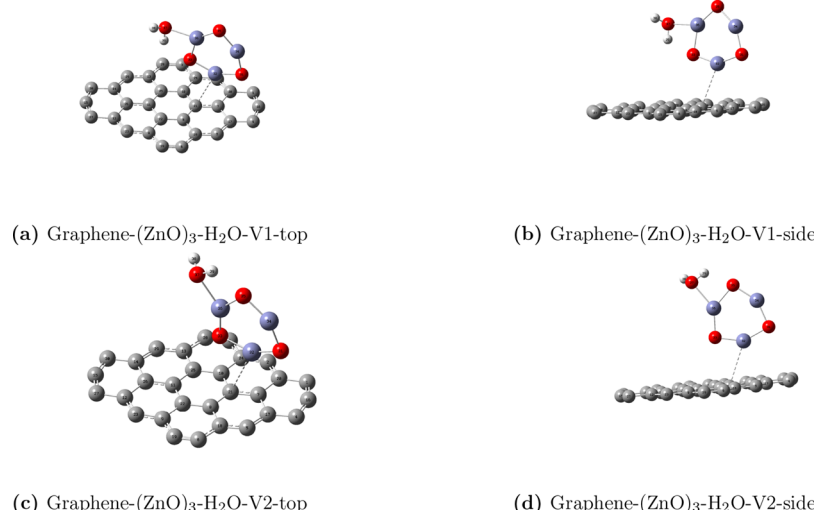


Figure 8. Optimized structures of H_2O adsorption on Graphene-(ZnO)3 system-vertical 1 (Zn–C bond) (a) pathway 1 top view, (b) pathway 1 side view, (c) pathway 2 top view, and (d) pathway 2 side view calculated using B3LYP/DGDZVP2.

Figure 9 shows the optimized structures of H_2O adsorption on $(\text{ZnO})_3$ anchored on GO1, GO2, GO4, and GO5 models. Each model has two different hydration and hydrolysis pathways, except for GO5 which has three. Water molecule adsorption energies in kcal/mol on a ZnO trimer already deposited on graphene were calculated using

$$E_{\text{Ad}4} = E_{\text{Tot}} - (E_{\text{Graphene}} + E_{\text{ZnO}} + E_{\text{Water}}) \quad (8)$$

and the corresponding energies of adsorption of ZnO trimer attached to a functional group on GO were calculated likewise from

$$E_{\text{Ad}5} = E_{\text{Tot}} - (E_{\text{GO}} + E_{\text{ZnO}} + E_{\text{Water}}) \quad (9)$$

In eq 8, E_{Tot} is the energy of the system after adsorbing $(\text{ZnO})_3$ on graphene, and in eq 9, it is the energy of the system after the water molecule is adsorbed on $(\text{ZnO})_3$ bonded to the functional group of the GO model. The thermodynamic Gibbs free energy (ΔG) and enthalpy (ΔH) changes were calculated using the following relations,

$$\Delta G_{\text{reaction}} = G_{\text{Products}} - G_{\text{Reactants}} \quad (10)$$

$$\Delta H_{\text{reaction}} = H_{\text{Products}} - H_{\text{Reactants}} \quad (11)$$

and our results are presented in Table 6 together with the HOMO–LUMO gap in the singlet state before and after the addition of one water molecule. Again the energies and free energies of adsorption in the triplet state are more negative than in the singlet state which is reflected in the total energy. Hydration is driven by the negative enthalpy change modulated by a substantial negative entropy contribution. Since DFT is a ground-state theory, calculations of the HOMO–LUMO gaps using this theory are subject to errors that are well-known, but our calculations using DFT should depict the trends in the HOMO–LUMO gap when the zinc oxide trimer is adsorbed on graphene or the functional groups of the GO models. The gap is substantially reduced from 4.42 eV for the bare Zinc oxide trimer to 1.21, 1.16, and 1.48 eV, respectively, for the zinc oxide trimer on GO2, GO3, and GO5, suggesting that GO models will be sensitive to light and electron promotion in the visible region.

Hydrolysis of Water at the Catalytic Sites of ZnO Trimmers.

In this section, we discuss the mechanistic pathways

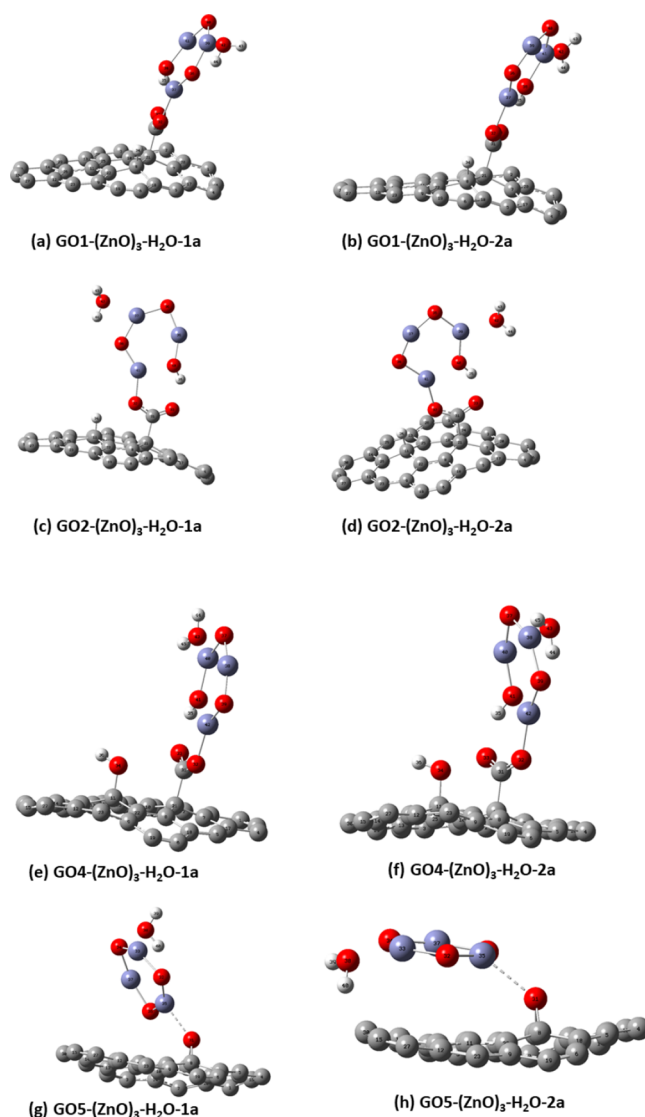


Figure 9. Optimized structures of H₂O absorption on (a) GO1-(ZnO)₃; pathway 1, (b) GO1-(ZnO)₃; pathway 2, (c) GO2-(ZnO)₃; pathway 1, (d) GO2-(ZnO)₃; pathway 2, (e) GO4-(ZnO)₃; pathway 1, (f) GO4-(ZnO)₃; pathway 2, (g) GO5-(ZnO)₃; pathway 1, and (h) GO5-(ZnO)₃; pathway 2 calculated using B3LYP/DGDZVP2 level of theory.

Table 6. Water Molecule Adsorption Energy and ΔG and ΔH Values in the Singlet and Triplet States and Energy Gap $\Delta E_{\text{HOMO-LUMO}}$ in the Singlet State^a

system	E_{Ad} in kcal/mol		ΔG in kcal/mol		ΔH in kcal/mol		$\Delta E(\text{HOMO-LUMO})$
	singlet	triplet	singlet	triplet	singlet	triplet	in eV
B3LYP/DGDZVP2							
(ZnO) ₃ + H ₂ O	-19.19	-18.95	-8.24	-8.14	-17.55	-17.26	4.65 (4.42)
(ZnO) ₃ -graphene + H ₂ O-vertical 1-pathway 1	-23.78	-107.68	-4.62	-83.80	-21.68	-103.29	1.46 (1.45)
(ZnO) ₃ -graphene + H ₂ O-vertical 1-pathway 2	-25.10	-107.73	-5.60	-84.19	-23.01	-103.55	1.45 (1.45)
(ZnO) ₃ -GO1 + H ₂ O-pathway 1	-70.29	-124.75	-48.45	-100.99	-67.79	-122.76	1.42 (1.41)
(ZnO) ₃ -GO1 + H ₂ O-pathway 2	-74.44	-127.64	-53.15	-104.17	-71.93	-125.17	1.44 (1.41)
(ZnO) ₃ -GO2 + H ₂ O-pathway 1	-69.44	-127.17	-47.94	-102.03	-67.13	-124.24	1.20 (1.22)
(ZnO) ₃ -GO2 + H ₂ O-pathway 2	-73.33	-130.34	-52.51	-106.27	-70.99	-127.41	1.19 (1.22)
(ZnO) ₃ -GO4 + H ₂ O-pathway 1	-74.77	-118.83	-53.69	-95.85	-71.76	-115.38	1.12 (1.16)
(ZnO) ₃ -GO4 + H ₂ O-pathway 2	-71.76	-115.38	-49.43	-91.81	-69.36	-113.67	1.14 (1.16)
(ZnO) ₃ -GO5 + H ₂ O-pathway 1	-30.63	-113.61	-9.25	-87.58	-27.85	-109.07	1.49 (1.48)
(ZnO) ₃ -GO5 + H ₂ O-pathway 2	-32.70	-116.89	-8.68	-87.57	-30.05	-112.33	1.22 (1.48)

^aThe HOMO–LUMO energy gaps of the models before water adsorption are shown in parenthesis.

and potential energy diagrams for hydrolysis in detail. The mechanisms were determined using the intrinsic reaction coordinate (IRC) method in the forward and reverse directions suggested by Fukui.⁴⁸ The hydrolysis of water molecules adsorbed on free ZnO trimers and on the same trimers adsorbed on graphene and the functional groups of the four graphene oxides GO1, GO2, GO4, and GO5 generally involve partial dissociation of the water and proton transfer to a neighboring oxygen atom on the zinc oxide trimer.

There are two vertical states 1 and 2 for the ZnO trimer adsorbed on graphene. Hydrolysis of water on ZnO trimer in the vertical 1 state of graphene C₃₀(ZnO)₃ does not proceed beyond the first water molecule when the hydrated structures effortlessly reorganize through an intermediate to the final stable hydrolyzed structure C₃₀O₃ZnO₂(OH)₂ with energies -167 kcal/mol in the singlet and -80.4 kcal/mole in the triplet state following curve crossing of the singlet and triplet states as displayed in Figure 10 and reported in Table 7. In contrast to this, successive hydration and hydrolysis of two water molecules in the vertical state 2 of the zinc oxide trimer on graphene shown in Figure 11 and recorded in Table 8 occurs readily with low activation energies for hydrolysis of 0.9 and 1.2 kcal/mol for the first hydrolysis and 26.3 and 2.7 kcal/mol for the second hydrolysis in the triplet and singlet states to respectively, without curve crossing, and the initial energy gap between triplet and singlet states is reduced from -45.5 kcal in the initial state to -31 kcal/mol in the final hydrolyzed product.

The trend of relatively low activation energies for the first and second hydrolysis of water molecules continues for the GO models even along different pathways although the structural intermediates may not be the same. This is illustrated in Figures 12, 13, 14, 15, and 16 that display the mechanistic pathways and the corresponding Tables 9 and 10 that record the associated energies for hydration and hydrolysis. Substantial bottlenecks in water splitting begin with the next few steps after hydrolysis.

Figures 12 and 13 show how the first water molecule is adsorbed and its oxygen atom bonds to one of two active Zn sites. Pathway 2 has lower negative adsorption energy in both singlet and triplet states than pathway 1. In contrast to Figure 12, Figure 13 shows a positive activation energy for the first hydrolysis reaction in both singlet and triplet states. The negative activation energy seen in Figure 12 may reflect the formation of an intermediate state rather than an activated state. The intermediate and/or activated state energies are small for

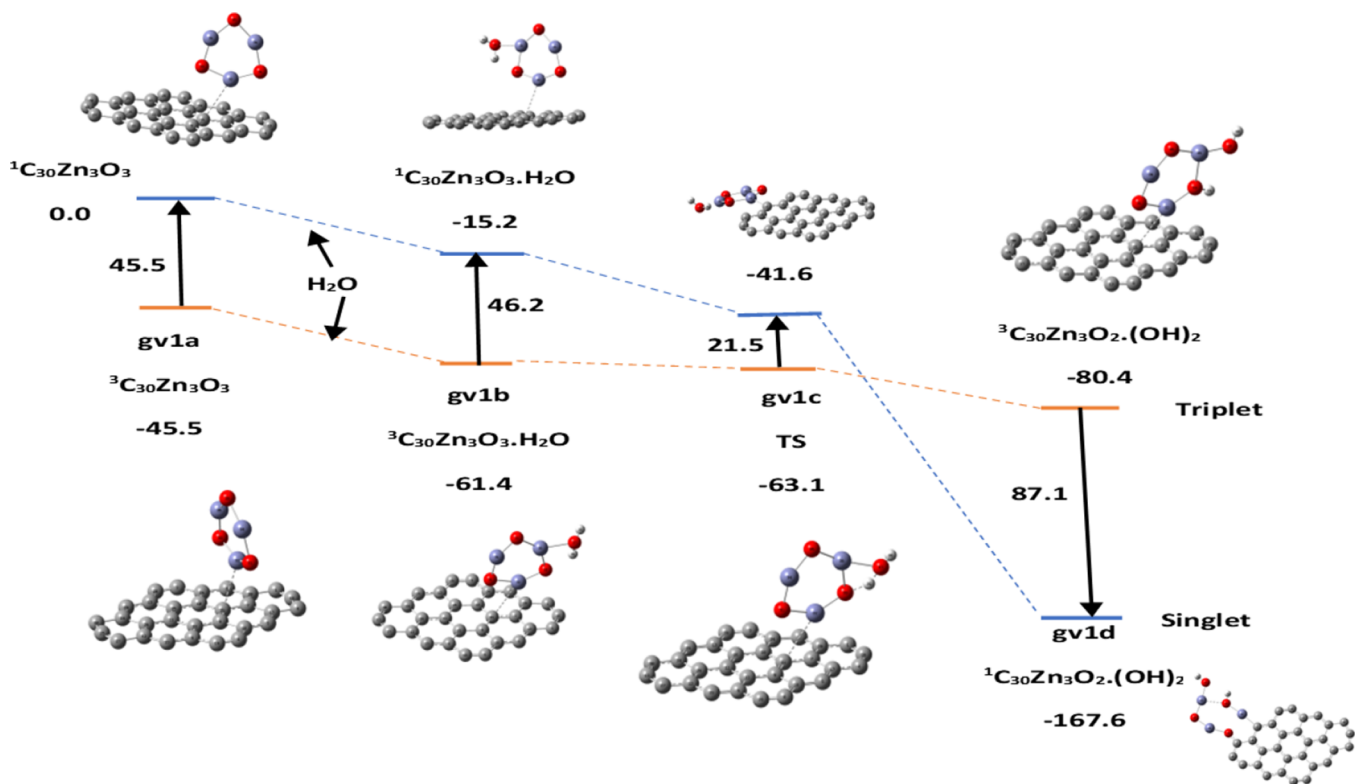


Figure 10. Hydrolysis pathway of one water molecule on $(\text{ZnO})_3$ deposited on graphene: vertical 1.

Table 7. Graphene [C₃₀] Vertical 1-Relative Energies in kcal/mol of the Adsorption and Hydrolysis of the First Water Molecule via an Intermediate (INT) or Transition State (TS) in Singlet and Triplet Spin Configurations Shown in Figure 10^a

	Zn ₃ O ₃	Zn ₃ O ₃ · H ₂ O	INT/TS	Zn ₃ O ₂ (OH) ₂
	gv1a	gv1b	gv1c	gv1d
E	0.0(S)	-15.2	-41.6	-167.69(T)
	-45.5(T)	-61.4	-63.1	-80.4(S)
E _{abs,reorg}		-15.5(S)	-26.4(S)	
		-15.9(T)	-1.7(T)	
freq			-42.3(S)	
			-883.3(T)	

^aThe temperature is 298 K.

both pathways. Along pathway 1, the molecular shapes of the first hydrolyzed products are distorted in the singlet and triplet states.

Table 9 shows the relative energies of the adsorption and hydrolysis of two water molecules on the GO1 model in two different pathways, corresponding to Figures 12 and 13. The transition state (TS) in each step is confirmed with the IRC calculation and has one negative frequency.

The GO2 and GO4 models show hydration and hydrolysis reaction pathways similar to the GO1 model. The PES for the hydration and hydrolysis of the GO2 and GO4 models with two water molecules and the relative energy values are shown in the SI document in Figures S5, S6, S7, S8, and Tables S28, and S29 respectively. The GO5 model has 2 vacant Zn sites to bind incoming water molecules as the $(\text{ZnO})_3$ is bound to the epoxy group of the GO5 model via one Zn atom of the $(\text{ZnO})_3$. Hence there are 3 possible reaction pathways for the hydrolysis reaction

with two water molecules as shown in Figures 14–16. The first hydrolysis reaction pathways 1a and 1b shown in Figures 14 and 15 are the same. When the second water molecule is adsorbed after the first hydrolysis reaction, the H atom can form a O–H bond with either one of the two O atoms on the ring adjacent to the binding site on the $(\text{ZnO})_3$. Table 10 shows the relative energies of the hydrolysis reactions of two water molecules for the GO5 model also displayed in Figures 14–16. Although the energies of all three reaction pathways are not significantly different, pathway 1b has comparatively lower transition states on both singlet and triplet states.

Table 11 summarizes the relative energies and energy changes of hydration and hydrolysis reaction of bare $(\text{ZnO})_3$ and $(\text{ZnO})_3$ on graphene and GO systems with two water molecules. From the table, it appears that graphene would not be a suitable substrate for water splitting in either of the vertical states V1 or V2. Hydrolysis is incomplete and is terminated after a single water molecule is hydrolyzed in the V1 state. The overall energy change for hydrolysis of a single water molecule on graphene is -167.76 kcal/mol in the V1 singlet spin configuration and -34.9 kcal/mol in the triplet spin configuration. The hydrolysis of water on the V1 graphene system is successful only in the triplet state. The hydrolysis reaction of $(\text{ZnO})_3$ on the vertical 2 graphene system occurs in both states with one water molecule but not with the second water molecule. This may be due to the hydrophobic property of the graphene sheet being transferred to the $(\text{ZnO})_3$ in the singlet state.

■ WATER SPLITTING

GO1 Model. In this section, we consider the final steps in the mechanism and energetics of water splitting on a GO model starting from the hydrolyzed product to produce H₂ and O₂

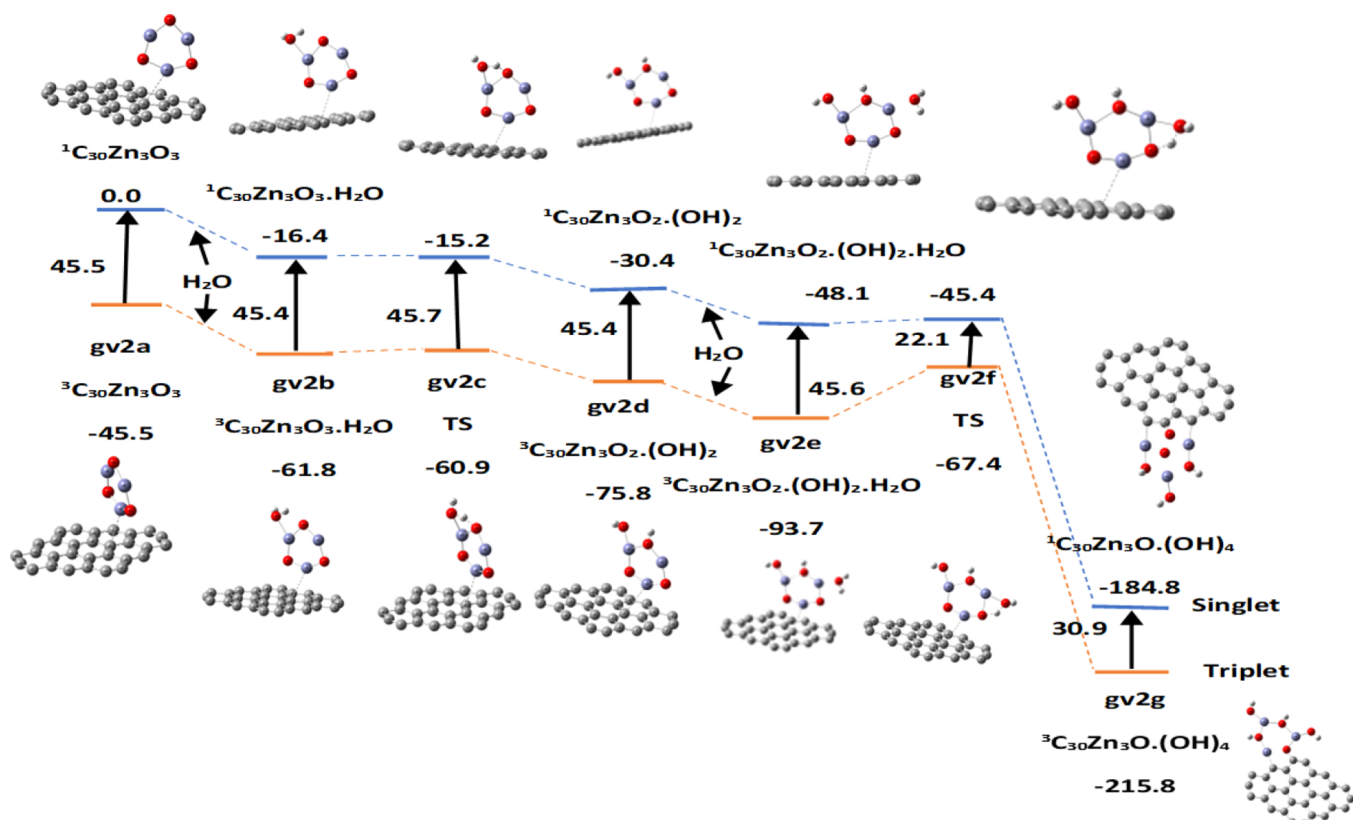


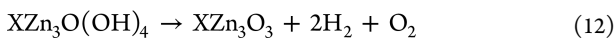
Figure 11. Hydrolysis pathway of one water molecule adsorbed on $(\text{ZnO})_3$ deposited on graphene: vertical 2.

Table 8. Graphene $[\text{C}_{30}]$ Vertical 2-Relative Energies in kcal/mol of the Adsorption and Hydrolysis of the First Water Molecule in Singlet and Triplet States Shown in Figure 11^a

	Zn_3O_3	$\text{Zn}_3\text{O}_3 \cdot \text{H}_2\text{O}$	TS	$\text{Zn}_3\text{O}_2(\text{OH})_2$	$\text{Zn}_3\text{O}_2(\text{OH})_2 \cdot \text{H}_2\text{O}$	TS	$\text{Zn}_3\text{O}(\text{OH})_4$
	gv2a	gv2b	gv2c	gv2d	gv2e	gv2f	gv2g
<i>E</i>	0.0(S) -45.5(T)	-16.4 -61.8	-15.2 -60.9	-30.4 -75.8	-48.1 -93.7	-45.4 -67.4	-184.8(S) -215.8(T)
<i>E_{abs,act}</i>		-16.4(S) -16.3(T)	1.2(S) 26.3(T)		-17.7(S) -17.8(T)	2.7(S) 26.6(T)	
freq			-913.8(S) -910.7(T)			-1059.4(S) -1064.7(T)	

^aThe temperature is 298 K.

using the cluster models as catalysts as shown in eq 12 where X denotes the GO model.



Here we will assume "X" to represent the GO1 model ($\text{C}_{31}\text{O}_2\text{H}_2$). This reaction is highly endothermic with an enthalpy change of 116 kcal/mol at 298 K. The intermediate steps in the reaction determine the overall rate of water splitting in the GO1 model as it was in our previous study of water splitting using the bare $(\text{ZnO})_3$ nanocatalyst. Figures 17 and 18 show the intermediate steps involved in the evolution of the first hydrogen molecule; the corresponding potential energy values are summarized in Tables 12 and 13. Clearly, the rate-determining step is the rearrangement of the intermediate. All transition states have negative frequency values as shown in the Tables 12 and 13.

The energy change for the rearrangement is ≈ 94.2 kcal/mol in the triplet and singlet states that corresponds to the energy difference between the structures GO1g1 and GO1i1. The

corresponding activation energies are ≈ 112.5 kcal/mol, showing that the transformation from the hydrolyzed product $\text{GO1Zn}_3\text{O}(\text{OH})_4$ to $\text{GO1HZn}_3\text{O}_2(\text{OH})_3$ is more likely the rate-determining step, as already observed for the bare $(\text{ZnO})_3$ nanocluster for which the rearrangement energies are 53.5 and 76.0 kcal/mol in the triplet and singlet states, with activation energies of 82.8 and 120.8 kcal/mol, respectively. The rearrangement energies in the singlet (76.0 kcal/mol) and triplet (53.5 kcal/mol) states of the bare ZnO trimer are smaller than for the $(\text{ZnO})_3$ -GO1 model (94.2 kcal/mol). The activation energy for this transformation on the bare ZnO trimer is lower in the singlet state (82.8 kcal/mol) but higher in the triplet state (120.8 kcal/mol) than for the $(\text{ZnO})_3$ -GO1 model in either state (112.5 kcal/mol).

After the first H_2 molecule is desorbed (Figure 17), the remaining 'H' atoms in the structure1 (GO1i1 in the Figure 17 in both the singlet and triplet states) are arranged favorably to form another H-H bond to produce the second H_2 molecule followed by the formation of an oxygen molecule in the triplet

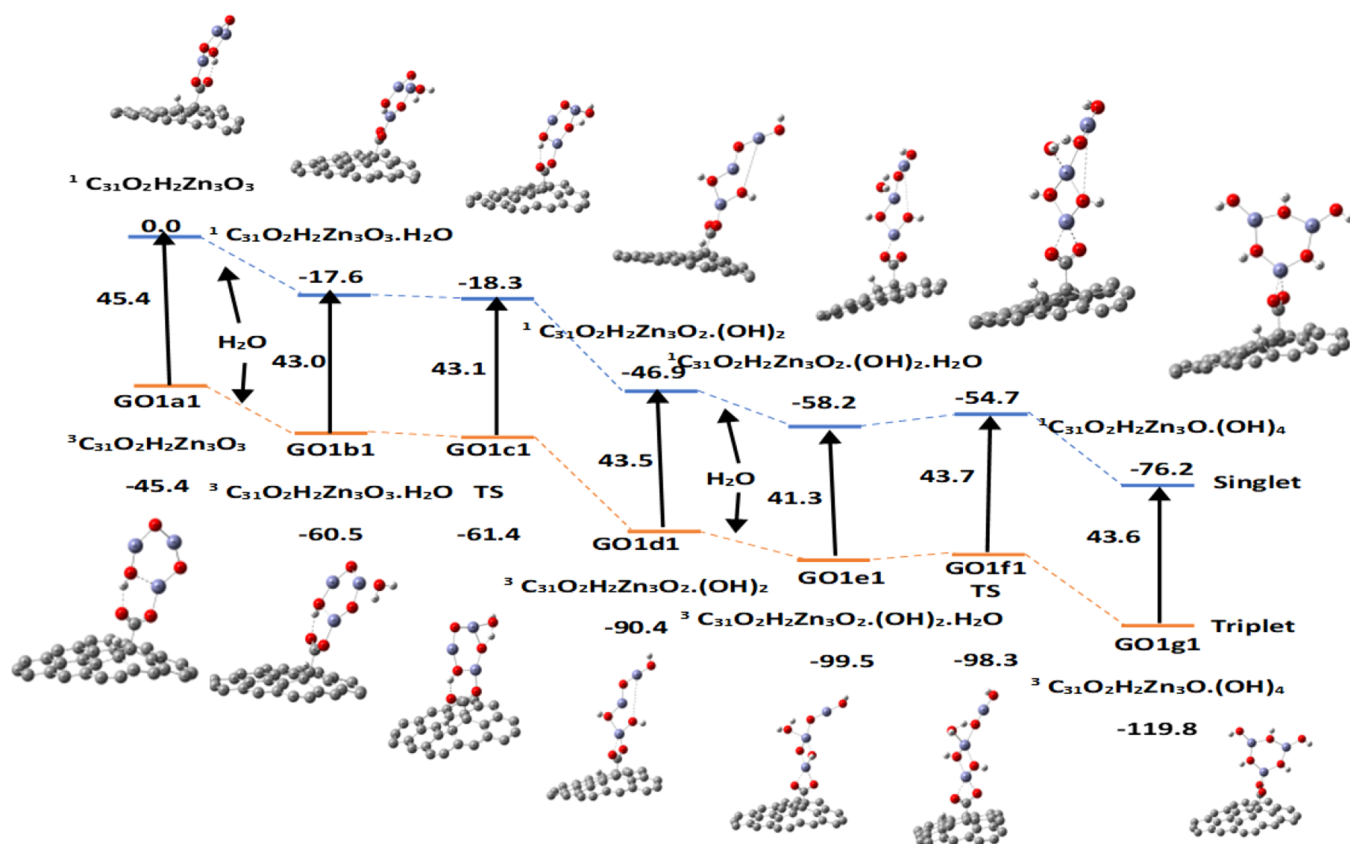


Figure 12. Potential energy surface (PES) for the hydration and hydrolysis of two water molecules on GO1: pathway 1, using B3LYP/DGDZVP2 level of theory. Relative energies in kcal/mol. The temperature is 298 K.

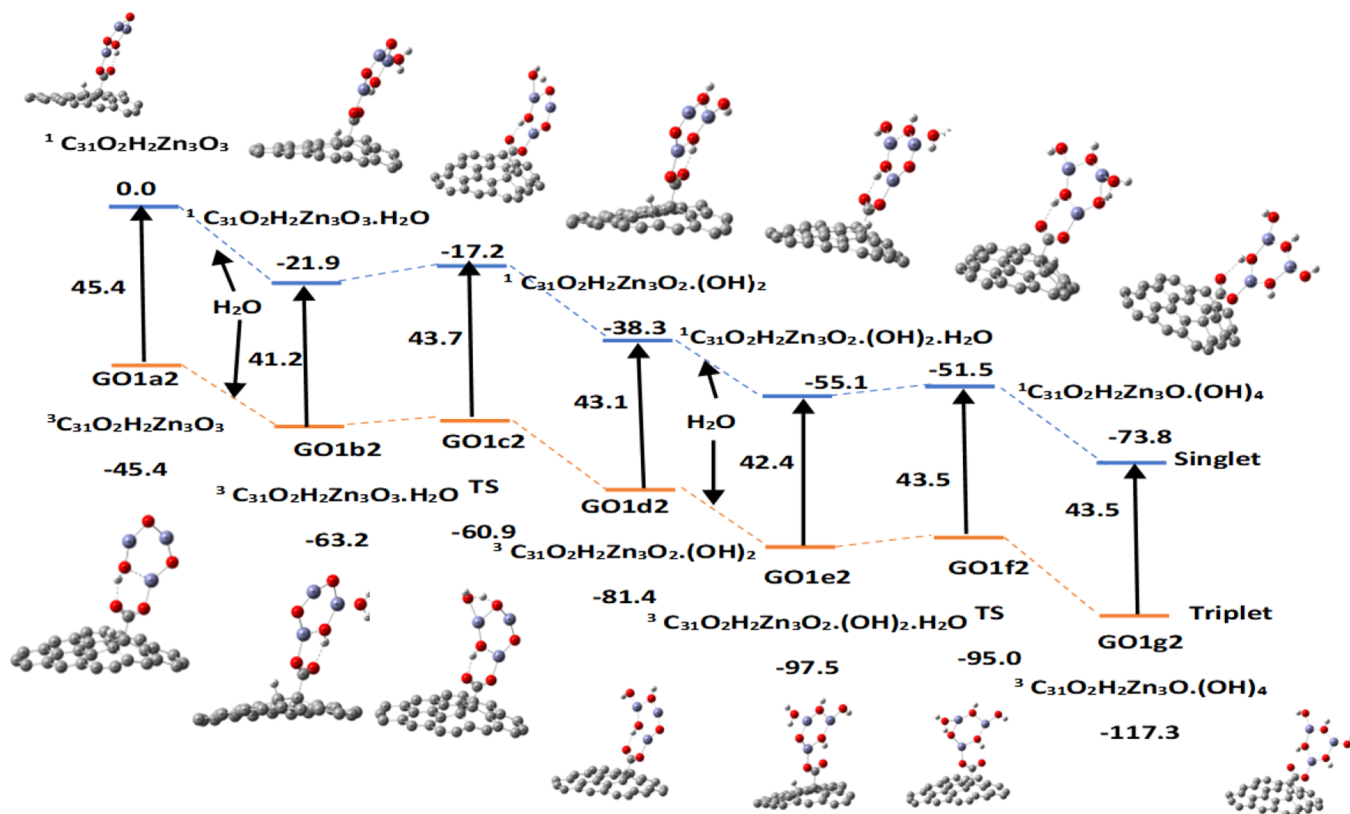


Figure 13. Potential energy surface (PES) for the hydration and hydrolysis of two water molecules on GO1: pathway 2, using B3LYP/DGDZVP2 level of theory. Relative energies in kcal/mol. The temperature is 298 K.

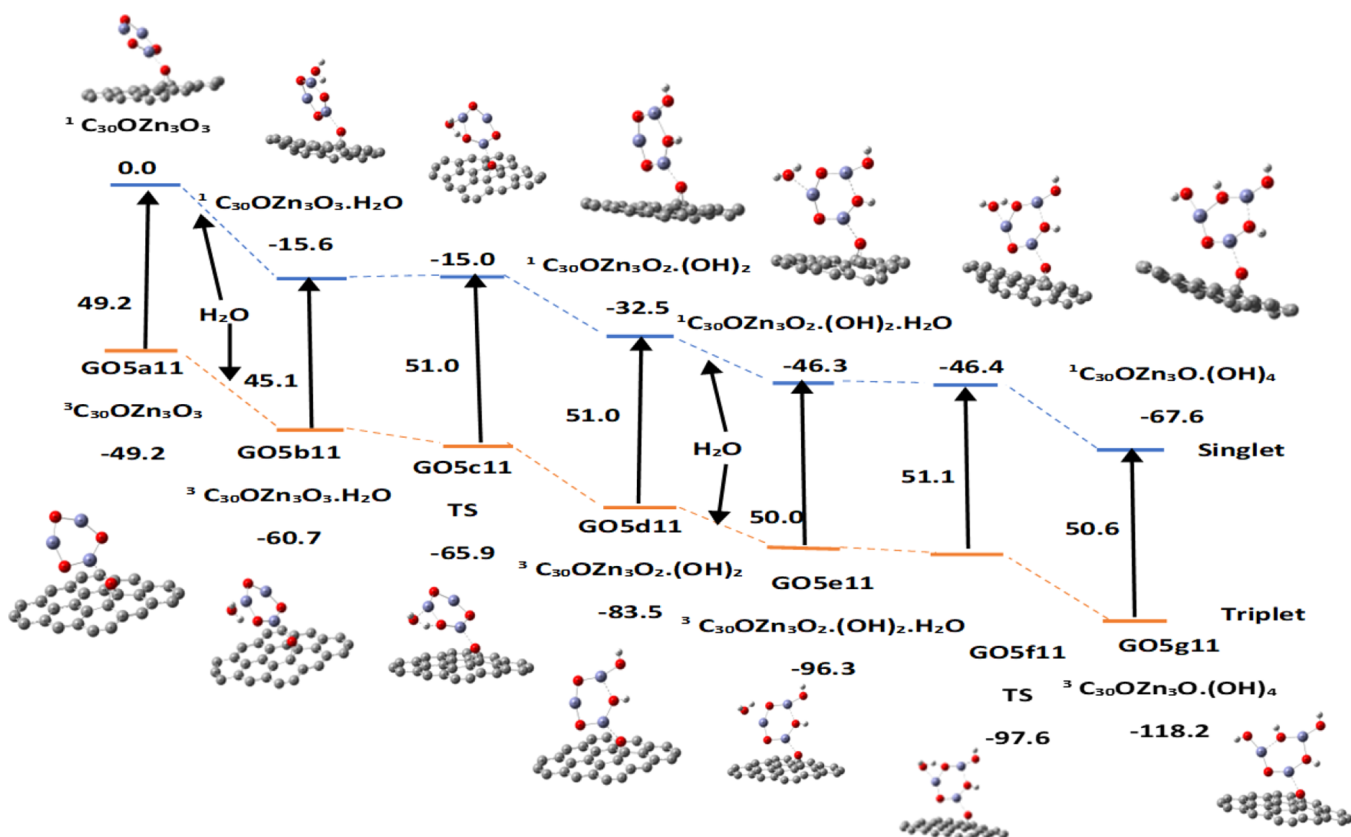


Figure 14. Potential energy surface (PES) for the hydration and hydrolysis of two water molecules on GO5: pathway 1a, using B3LYP/DGDZVP2 level of theory. Relative energies in kcal/mol.

Table 9. Relative Energies in kcal/mol of the Adsorption and Hydrolysis of the First and Second Water Molecules on GO1 [$\text{C}_3\text{O}_2\text{H}_2$] prior to Water Splitting on Singlet and Triplet States Shown in Figures 12 and 13^a

PW1	$\text{GO1Zn}_3\text{O}_3$	$\text{C}_3\text{O}_2\text{H}_2\text{Zn}_3\text{O}_3 \cdot \text{H}_2\text{O}$	INT/TS	$\text{GO1Zn}_3\text{O}_2(\text{OH})_2$	$\text{GO1Zn}_3\text{O}_2(\text{OH})_2 \cdot \text{H}_2\text{O}$	TS	$\text{GO1Zn}_3\text{O}(\text{OH})_4$
	GO1a1	GO1b1	GO1c1	GO1d1	GO1e1	GO1f1	GO1g1
E	0.0(S)	-17.6	-18.3	-46.9	-58.2	-54.7	-76.2(S)
	-45.4(T)	-60.5	-61.4	-90.4	-99.5	-98.3	-119.8(T)
$E_{\text{abs,act}}$		-17.6	-0.7(S)		-11.3	3.5	
		-15.1	-0.9(T)		-9.1	1.2	
freq			-702.7(S)			-958.1	
			-696.8(T)			-955.3	
PW2	GO1a2	GO1b2	GO1c2	GO1d2	GO1e2	GO1f2	GO1g2
E	0.0(S)	-21.9	-17.2	-38.3	-55.1	-51.5	-73.8(S)
	-45.4(T)	-63.2	-60.9	-81.4	-97.5	-95.0	-117.3(T)
$E_{\text{abs,act}}$		-21.9	4.7(S)		-16.8	3.6	
		-17.8	2.3(T)		-16.1	2.5	
freq			-1051.4(S)			-1089.9	
			-1042.7(T)			-1086.2	

^aThe temperature is 298 K.

state and restoring the GO1 catalysts to their original triplet or singlet states as shown in Figure 18. This sequence eliminates the need for the structures m and n that are present in the reaction pathway for water splitting on the bare $(\text{ZnO})_3$ nanocluster catalyst.

Figure 19 compares the water splitting reaction on bare $(\text{ZnO})_3$ and GO1- $(\text{ZnO})_3$ system. The singlet and triplet states of bare $(\text{ZnO})_3$ and the GO1- $(\text{ZnO})_3$ systems are represented in blue, orange, grey, and yellow color lines, respectively. The triplet state of GO1- $(\text{ZnO})_3$ has the lowest energy. This is

similar to an oxygen molecule for which the triplet state has a lower energy than the singlet state. The point here is that the singlet-triplet order for the bare zinc oxide trimer is reversed when the zinc oxide trimer is adsorbed on graphene or on any one of the GO models. This may be an artifact of the use of DFT for both states or caused our modeling of the triplet state as a singlet state with $S = 1$, spin contamination in graphene-based systems, or by a spin configuration of the molecular orbitals unknown to us. The singlet and triplet states in both systems have similar arrangements during the first H_2 desorption.

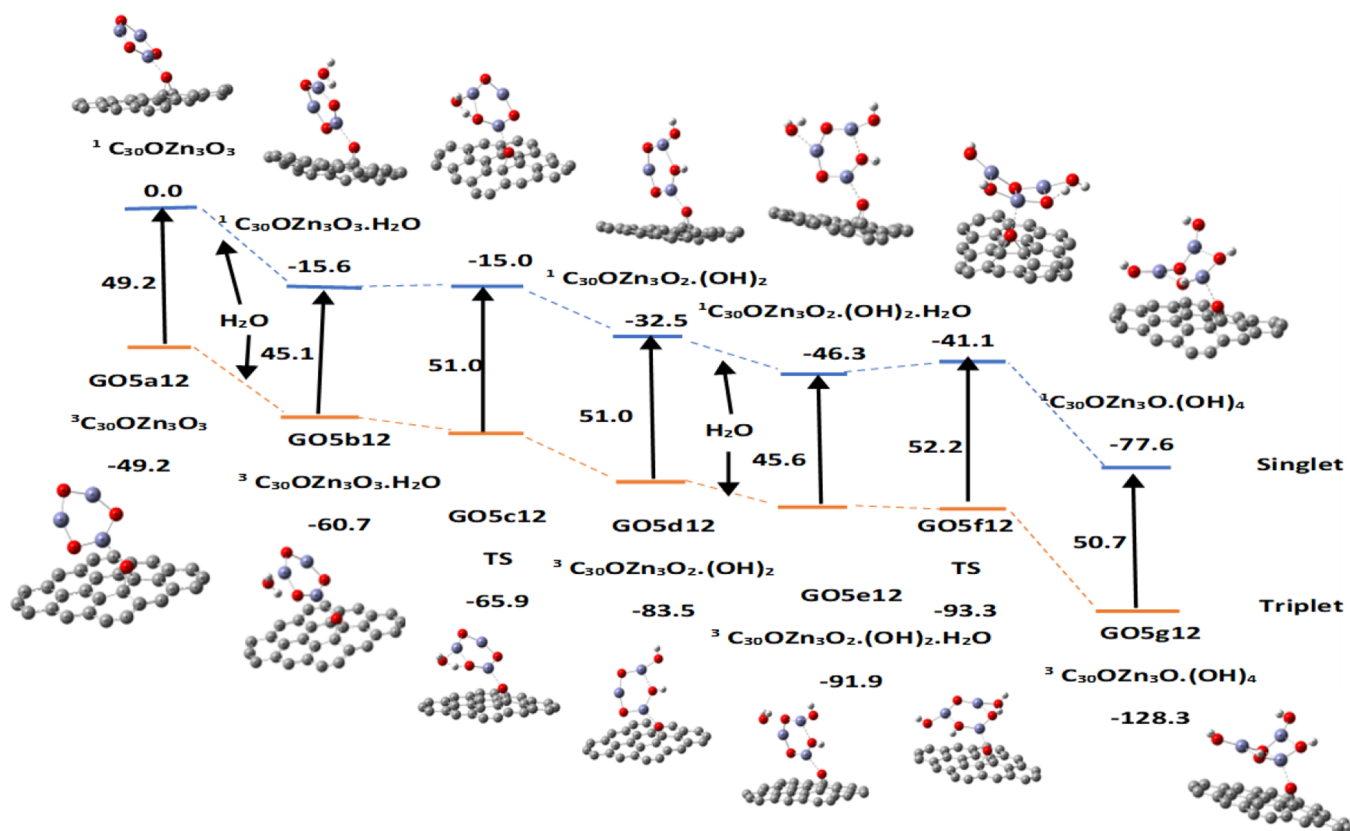


Figure 15. Potential energy surface (PES) for the hydration and hydrolysis of two water molecules on GO5: pathway 1b, using B3LYP/DGDZVP2 level of theory. Relative energies in kcal/mol.

Table 10. GO5[C_{30}O]-Relative Energies in kcal/mol of the Formation and Release of the First Hydrogen Molecule during Water Splitting Shown in Figures 14–16^a

PW1a	GO5Zn ₃ O ₃	GO5Zn ₃ O ₃ · H ₂ O	INT/TS	GO5Zn ₃ O ₂ (OH) ₂	GO5Zn ₃ O ₂ (OH) ₂ · H ₂ O	INT/TS	GO5g11
	GO5a11	GO5b11	GO5c11	GO5d11	GO5e11	GO5f11	
E	0.0(S)	-15.6	-15.0	-32.5	-46.3	-46.4	-67.6(S)
	-49.2(T)	-60.7	-65.9	-83.5	-96.3	-97.6	-118.2(T)
$E_{\text{abs,act}}$		-15.6	0.6(S)		-13.8	-0.1	
		-11.5	-5.2(T)		-12.8	-1.3	
freq			-934.9(S)			-678.2	
			-843.8(T)			-786.7	
PW1b	GO5a12	GO5b12	GO5c12	GO5d12	GO5e12	GO5f12	GO5g12
E	0.0(S)	-15.6	-15.0	-32.5	-46.3	-41.1	-77.6(S)
	-49.2(T)	-60.7	-65.9	-83.5	-91.9	-93.3	-128.3(T)
$E_{\text{abs,act}}$		-15.6	0.6(S)		-13.8	5.2	
		-11.5	-5.2(T)		-8.4	1.4	
freq			-934.9(S)			-456.1	
			-843.8(T)			-975.1	
PW2	GO5a2	GO5b2	GO5c2	GO5d2	GO5e2	GO5f2	GO5g2
E	0.0(S)	-17.5	-14.8	-29.8	-45.9	-44.1	-66.9(S)
	-49.2(T)	-63.6	-64.7	-80.5	-89.5	-93.8	-116.9(T)
$E_{\text{abs,act}}$		-17.5	2.7(S)		-16.1	1.8	
		-14.4	-1.1(T)		-9.0	-4.3	
freq			-887.2(S)			-994.3	
			-856.0(T)			-1008.1	

^aThe temperature is 298 K.

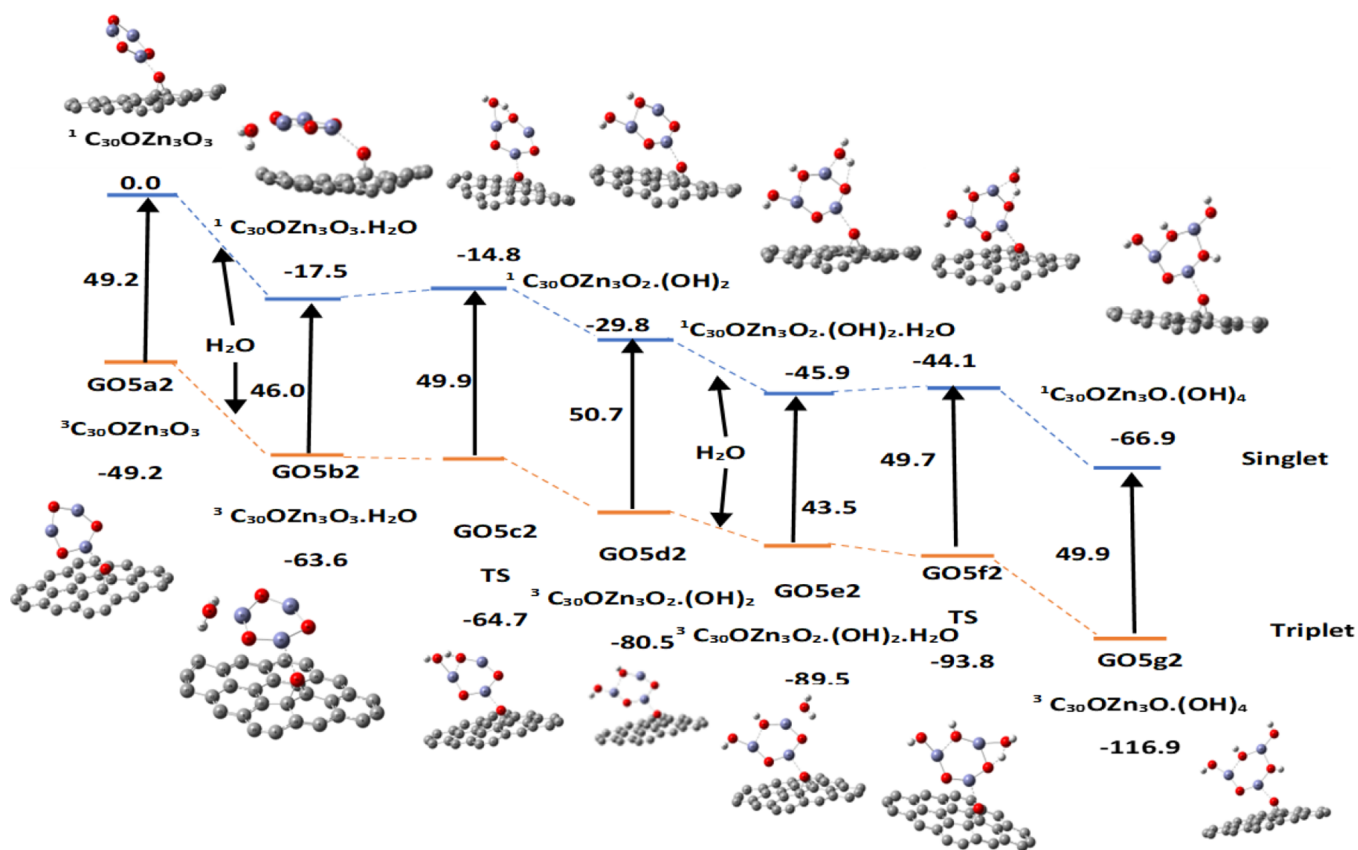


Figure 16. Potential energy surface (PES) for the hydration and hydrolysis of two water molecules on GO5: pathway 2, using B3LYP/DGDZVP2 level of theory. Relative energies in kcal/mol.

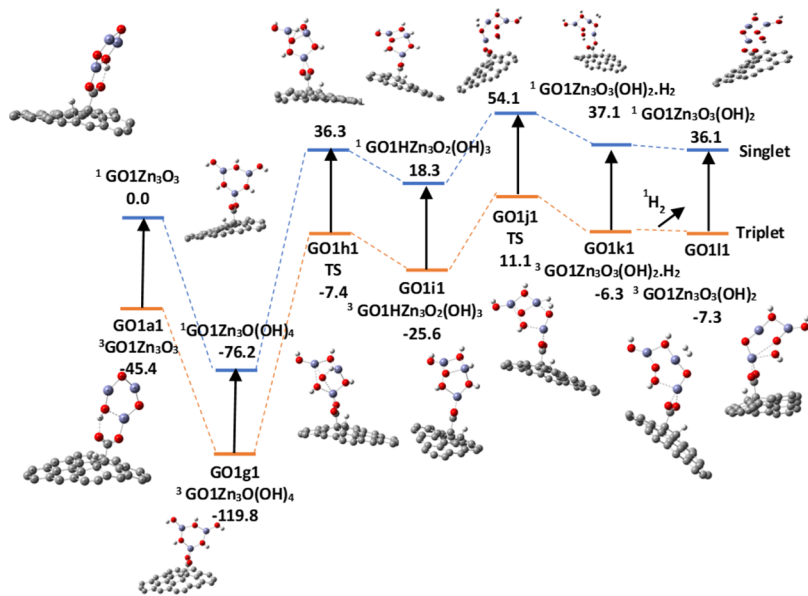


Figure 17. Water splitting reaction on GO1 $[\text{C}_{31}\text{O}_2\text{H}_2]$ toward the formation and desorption of the first H_2 : pathway 1.

Table 11. Relative Energies and Energy Changes of Hydration and Hydrolysis of $(\text{ZnO})_3$ on Different Systems, S(0) = Singlet and S(1) = Triplet

system		E_{bare}	E_{hydro1}	ΔE_{hydro1}	E_{hydro2}	ΔE_{hydro2}	
$(\text{ZnO})_3$							
	path a S(1)	57.5	11.3	-42.3	-14.9	-72.4	Table 4 ³⁹
	S(0)	0.0	-31.2	-31.2	-78.3	-78.3	Table 4 ³⁹
	path b1	57.5	11.3	-42.3	-14.7	-72.2	
		0.0	-31.2	-31.2	-79.9	-79.7	
	path b2	57.5	11.3		-14.7	-72.4	Table 4 ³⁹
		0.0	-31.2		-78.3	-78.3	
GV1	V1 singlet S(0)	0	-167.6	-167.6	NA	NA	Table 7
	triplet S(1)	-45.5	-80.5	-34.9	NA	NA	
GV2	V2(S0)	0.0	-30.4	-30.4	-184.8	-184.8	Table 8
	S(1)	-45.5	-75.8	-30.3	-215.8	-170.3	
GO1	P1 S(0)	0.0	-46.9	-46.9	-76.2	-76.2	Table 9
	S(1)	-45.4	38.3	-45	-119.8	-74.4	
	P2 S(0)	0.0	-38.3	-38.3	-73.8	-73.8	
	S(1)	-45.4	-81.4	-35.9	117.3	-71.9	
GO2	P1 S(0)	0.0	-47.4	-47.4	-76.6	-76.6	Table S28
	S(1)	-49.6	-99.7	-50.1	-128.7	-79.1	
	P2 S(0)	0.0	-38.4	-38.4	-73.6	-73.6	
	S(1)	-49.6	-89.1	-39.5	-123.8	-74.2	
GO4	P1 (S0)	0.0	-38.4	-38.4	-74.3	-74.3	Table S29
	S(1)	-49.2	-76.2	-26.2	-121.9	-72.7	
	P2 S(0)	0.0	-46.3	-46.3	-76	-76	
	S(1)	-49.2	-99.2	-50	-126.8	-77.6	
GO5	P1a S(0)	0.0	-32.5	-32.5	-67.6	-67.6	Table 10
	S(1)	-49.2	-83.5	-50.1	-118.2	-69	
	P1b S(0)	0.0	-46.3	-46.3	77.6	-77.6	Table 10
	S(1)	-49.2	-99.2	-50	-128.3	-79.1	
	P2 S(0)	0.0	-29.8	-29.8	-66.9	-66.9	Table 10
	S(1)	-49.2	-80.5	-31.3	-116.9	-67.7	

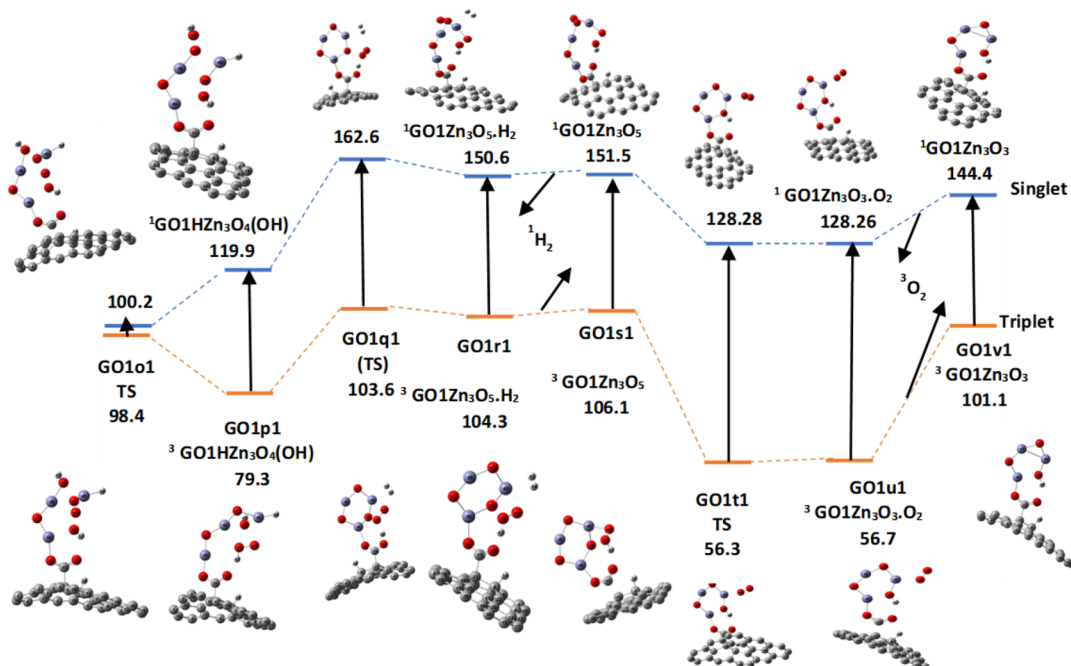
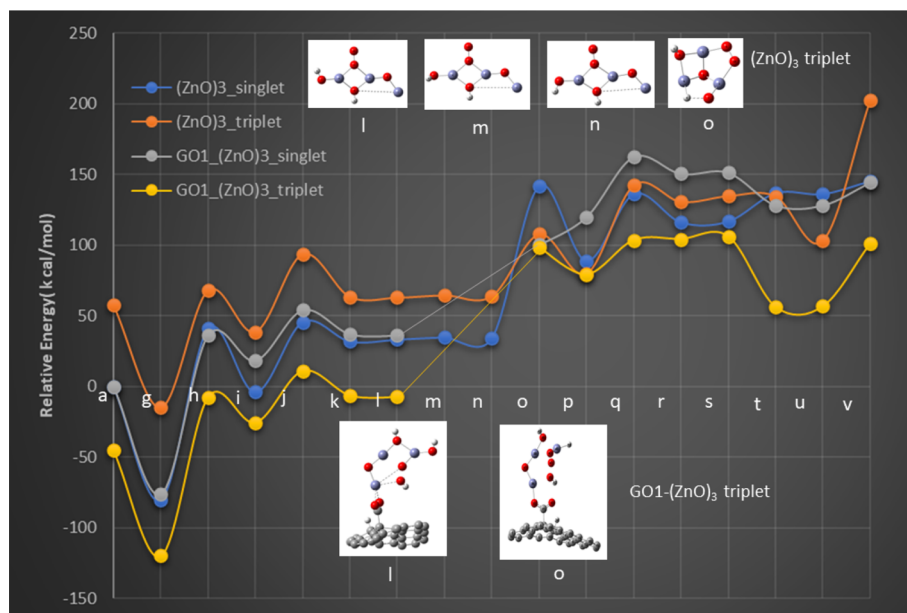
**Figure 18.** Water splitting on $\text{GO1}[\text{C}_{31}\text{O}_2\text{H}_2]$ toward the formation and desorption of the second H_2 and O_2 ; pathway 1.

Table 12. Relative Energies in kcal/mol of the Formation and Release of the First Hydrogen Molecule during Water Splitting on GO1 Model Shown in Figure 17^a

pathway 1	GO1Zn ₃ O(OH) ₄	TS	HZn ₃ O ₂ (OH) ₃	TS	Zn ₃ O ₃ (OH) ₂ · H ₂	Zn ₃ O ₃ (OH) ₂	TS
	GO1g1	GO1h1	GO1i1	GO1j1	GO1k1	GO1l1	GO1m1
E	-76.2	36.3	18.3	54.1	37.1	36.1	NA
	-119.8	-7.4	-25.6	11.1	-6.3	-7.3	NA
E _{ad,act}	-76.2	112.5(S)		35.8			
	-74.4	112.4(T)		36.7			
freq		-684.1		-1237.3			
		-687.5		-1235.1			

^aThe temperature is 298 K.**Table 13.** Relative Energies in kcal/mol of the Formation and Release of the Second Hydrogen Molecule Followed By an Oxygen Molecule Completing Water Splitting on GO1 Model Is Shown in Figure 18^a

pathway 1	GO1Zn ₃ O ₃ (OH) ₂	TS	GO1HZn ₃ O ₄ (OH)	TS	GO1Zn ₃ O ₅ · H ₂	GO1Zn ₃ O ₅	INT	GO1Zn ₃ O ₃ · O ₂	GO1Zn ₃ O ₃
	GO1n1	GO1o1	GO1p1	GO1q1	GO1r1	GO1s1	GO1t1	GO1u1	GO1v1
E	NA	100.2(S)	119.9	162.6	150.6	151.5	128.28	128.26	144.4(S)
	NA	98.4(T)	79.3	103.5	104.3	106.1	56.3	56.7	101.1(T)
E _{ad,act}	NA	64.1(S)		42.7			-23.3(S)		
	NA	105.7(T)		24.3			-49.8(T)		
freq		-65.2		-27.5			-29.8		
		-43.6		-1104.7			-26.7		

^aThe temperature is 298 K.**Figure 19.** Schematic comparison of water splitting reaction on bare (ZnO)₃ and GO1[(C₃₁O₂H₂)₃] toward the formation and desorption of 2H₂ and O₂: pathway 1.

However, the GO1-(ZnO)₃ model skips two steps (structures m and n) in the second H₂ desorption. The singlet–triplet states cross during the O₂ desorption on bare (ZnO)₃ but not in the GO1-(ZnO)₃ system.

CONCLUSIONS

We have investigated the use of graphene and graphene-based metal oxides as substrates for metal oxide photocatalysts in water-splitting reactions using (ZnO)₃ nanoclusters as the metal oxide catalyst following our previous study of the same metal oxide nanocluster in the absence of a substrate.³⁹ The HOMO–

LUMO gap decreases from 4.47 eV for the bare (ZnO)₃ nanocluster to 1.41, 1.22, 1.26, and 1.48 eV for the (ZnO)₃ nanocluster attached to the respective graphene oxides GO1, GO2, GO4, and GO5 deposited on graphene sheets. The π structure of GO's apparently shows greater electron mobility and that could enhance the photocatalytic performance of (ZnO)₃ nanoclusters by increasing the electron–hole separation. The hydration and hydrolysis reaction of the (ZnO)₃ nanoclusters adsorbed on graphene and GO models were studied in both singlet and triplet states with the B3LYP/DGDZVP2 exchange functionals and basis sets in the gas phase

used by us previously in the absence of a substrate.³⁹ The GO1, GO2, and GO4 exhibit two different reaction pathways for hydrolysis, and the GO5 model has three hydrolysis pathways since the Zn atom of the nanocluster binds preferentially with the O atom in the epoxy group. The energy barriers for both hydration and hydrolysis are low compared to the barriers for the successive formation of two singlet hydrogen molecules followed by the production of a triplet oxygen molecule in the overall splitting of two water molecules as shown in eq 1. The triplet state of GO1-(ZnO)₃ has the lowest relative energy compared to the bare (ZnO)₃. The water splitting reaction pathway with GO1-(ZnO)₃ catalyst skips two steps, “m” and “n,” that were present in the absence of a substrate since the step preceding “m” is already in a favorable conformation to split water to produce two H₂ molecules followed by an oxygen molecule. Increasing the number of water molecules to more than two, as in the presence of a water layer or in solution, could alter the potential energy profiles, energy barriers, and dynamics of water splitting from what we observe in the gas phase due to the presence of an extended hydrogen-bonded network on the catalytic surface and interactions with water molecules and hydrogen and hydroxide ions further beyond the surface reported in similar systems.⁴⁹ We conclude that the ZnO trimer and larger ZnO n-mers ($n > 3$) deposited on GO systems are potentially attractive subjects for further investigation as catalysts for water splitting. The calculations of the PES using the IRC method are slow and limited in scope, and faster ab-initio calculations of the dynamics of water splitting would be interesting.

ASSOCIATED CONTENT

Supporting Information

The Supporting Information is available free of charge at <https://pubs.acs.org/doi/10.1021/acsomega.3c04882>.

A detailed description of the properties and HOMO, LUMO images of each structure in both singlet and triplet states, IR spectra of H₂O adsorption of GO1-(ZnO)₃ system along different pathways, PES, and the related energies for the reaction of hydration and hydrolysis of H₂O molecules on GO2-(ZnO)₃ and GO4-(ZnO)₃ systems (PDF)

AUTHOR INFORMATION

Corresponding Authors

Duwage C. Perera – Department of Chemistry, University of Maine, Orono, Maine 04469, United States;  orcid.org/0000-0003-4237-138X; Email: charitha.perera@maine.edu

Jayendran C. Rasaiah – Department of Chemistry, University of Maine, Orono, Maine 04469, United States;  orcid.org/0000-0002-4453-7438; Email: rashaiah@maine.edu

Complete contact information is available at:

<https://pubs.acs.org/10.1021/acsomega.3c04882>

Notes

The authors declare no competing financial interest.

ACKNOWLEDGMENTS

The authors thank Stephen Cousins, Bruce Segee, and the staff of the University of Maine High-Performance Computing (HPC) Group for the allotment of computer time. They thank Professor S. Vaiteeswaran for his helpful comments, Dr. Chris Mundy of the Pacific Northwest National Lab for serving on the

first authors thesis committee, and Eric Lovejoy for technical assistance. The computer resources used in this study were supported by an NSF grant CC* Comp High-Memory Computer Resources for Maine, Award Number: 2018851. They also thank the referees for critical reviews of the manuscript.

REFERENCES

- (1) Fujishima, A.; Honda, K. Electrochemical Photolysis of Water at a Semiconductor Electrode. *Nature* **1972**, *238*, 37–38.
- (2) Razek, S. A.; Popeil, M. R.; Wangoh, L.; Rana, J.; Suwandalatne, N.; Andrews, J. L.; Watson, D. F.; Banerjee, S.; Piper, L. F. J. Designing catalysts for water splitting based on electronic structure considerations. *Electron. Struct.* **2020**, *2*, No. 023001.
- (3) Eidsvåg, H.; Bentouba, S.; Vajeeston, P.; Yohi, S.; Velauthapillai, D. TiO₂ as a Photocatalyst for Water Splitting—An Experimental and Theoretical Review. *Molecules* **2021**, *26*, 1687.
- (4) Li, D.; Liu, H.; Feng, L. A Review on Advanced FeNi-Based Catalysts for Water Splitting Reaction. *Energy Fuels* **2020**, *34*, 13491–13522.
- (5) Galińska, A.; Walendziewski, J. Photocatalytic Water Splitting over Pt-TiO₂ in the Presence of Sacrificial Reagents. *Energy Fuels* **2005**, *19*, 1143–1147.
- (6) Fang, Z.; Dixon, D. A. Computational Study of H₂ and O₂ Production from Water Splitting by Small (MO₂)_n Clusters (M = Ti, Zr, Hf). *J. Phys. Chem. A* **2013**, *117*, 3539–3555.
- (7) Du, X.; Skachko, I.; Barker, A.; Andrei, E. Y. Approaching ballistic transport in suspended graphene. *Nat. Nanotechnol.* **2008**, *3*, 491–495.
- (8) An, X.; Yu, J. C. Graphene-based photocatalytic composites. *RSC Adv.* **2011**, *1*, 1426–1434.
- (9) Xiang, Q.; Yu, J.; Jaroniec, M. Graphene-based semiconductor photocatalysts. *Chem. Soc. Rev.* **2012**, *41*, 782–796.
- (10) Zhang, N.; Zhang, Y.; Xu, Y.-J. Recent progress on graphene-based photocatalysts: current status and future perspectives. *Nanoscale* **2012**, *4*, 5792–5813.
- (11) Han, L.; Wang, P.; Dong, S. Progress in graphene-based photoactive nanocomposites as a promising class of photocatalyst. *Nanoscale* **2012**, *4*, 5814–5825.
- (12) Zhu, Z.; Su, M.; Ma, L.; Ma, L.; Liu, D.; Wang, Z. Preparation of graphene oxide–silver nanoparticle nanohybrids with highly antibacterial capability. *Talanta* **2013**, *117*, 449–455.
- (13) Tang, J.; Chen, Q.; Xu, L.; Zhang, S.; Feng, L.; Cheng, L.; Xu, H.; Liu, Z.; Peng, R. Graphene Oxide–Silver Nanocomposite As a Highly Effective Antibacterial Agent with Species-Specific Mechanisms. *ACS Appl. Mater. Interfaces* **2013**, *5*, 3867–3874.
- (14) Cobos, M.; De-La-Pinta, I.; Quindós, G.; Fernández, M. J.; Fernández, M. D. Synthesis, Physical, Mechanical and Antibacterial Properties of Nanocomposites Based on Poly(vinyl alcohol)/Graphene Oxide–Silver Nanoparticles. *Polymer* **2020**, *12*, 723.
- (15) Zang, Z.; Zeng, X.; Wang, M.; Hu, W.; Liu, C.; Tang, X. Tunable photoluminescence of water-soluble AgInZnS–graphene oxide (GO) nanocomposites and their application in-vivo bioimaging. *Sens. Actuators, B* **2017**, *252*, 1179–1186.
- (16) Chen, D.; Feng, H.; Li, J. Graphene Oxide: Preparation, Functionalization, and Electrochemical Applications. *Chem. Rev.* **2012**, *112*, 6027–6053.
- (17) Standley, B.; Mendez, A.; Schmidgall, E.; Bockrath, M. Graphene-graphite oxide field-effect transistors. *Nano Lett.* **2012**, *12*, 1165–1169.
- (18) Dideikin, A. T.; Vul', A. Y. Graphene Oxide and Derivatives: The Place in Graphene Family. *Front. Phys.* **2019**, *6*, 149.
- (19) Georgakilas, V.; Tiwari, J. N.; Kemp, K. C.; Perman, J. A.; Bourlinos, A. B.; Kim, K. S.; Zboril, R. Noncovalent Functionalization of Graphene and Graphene Oxide for Energy Materials, Biosensing, Catalytic, and Biomedical Applications. *Chem. Rev.* **2016**, *116*, 5464–5519.
- (20) Khan, M.; Tahir, M. N.; Adil, S. F.; Khan, H. U.; Siddiqui, M. R. H.; Al-warthan, A. A.; Tremel, W. Graphene based metal and metal

- oxide nanocomposites: synthesis, properties and their applications. *J. Mater. Chem. A* **2015**, *3*, 18753–18808.
- (21) Parnianchi, F.; Nazari, M.; Maleki, J.; Mohebi, M. Combination of graphene and graphene oxide with metal and metal oxide nanoparticles in fabrication of electrochemical enzymatic biosensors. *Int. Nano Lett.* **2018**, *8*, 229–239.
- (22) Zhang, H.; Wang, X.; Li, N.; Xia, J.; Meng, Q.; Ding, J.; Lu, J. Synthesis and characterization of TiO₂/graphene oxide nanocomposites for photoreduction of heavy metal ions in reverse osmosis concentrate. *RSC Adv.* **2018**, *8*, 34241–34251.
- (23) Martins, P.; Ferreira, C.; Silva, A.; Magalhães, B.; Alves, M.; Pereira, L.; Marques, P.; Melle-Franco, M.; Lanceros-Méndez, S. TiO₂/graphene and TiO₂/graphene oxide nanocomposites for photocatalytic applications: A computer modeling and experimental study. *Composites, Part B* **2018**, *145*, 39–46.
- (24) Tayel, A.; Ramadan, A. R.; El Seoud, O. A. Titanium Dioxide/Graphene and Titanium Dioxide/Graphene Oxide Nanocomposites: Synthesis, Characterization and Photocatalytic Applications for Water Decontamination. *Catalysts* **2018**, *8*, 491.
- (25) Do, H. H.; Nguyen, D. L. T.; Nguyen, X. C.; Le, T.-H.; Nguyen, T. P.; Trinh, Q. T.; Ahn, S. H.; Vo, D.-V. N.; Kim, S. Y.; Le, Q. V. Recent progress in TiO₂-based photocatalysts for hydrogen evolution reaction: A review. *Arabian J. Chem.* **2020**, *13*, 3653–3671.
- (26) Yeh, T.-F.; Cihlář, J.; Chang, C.-Y.; Cheng, C.; Teng, H. Roles of graphene oxide in photocatalytic water splitting. *Mater. Today* **2013**, *16*, 78–84.
- (27) Chen, C.; Cai, W.; Long, M.; Zhou, B.; Wu, Y.; Wu, D.; Feng, Y. Synthesis of Visible-Light Responsive Graphene Oxide/TiO₂ Composites with p/n Heterojunction. *ACS Nano* **2010**, *4*, 6425–6432.
- (28) Ahn, B. D.; Kang, H. S.; Kim, J. H.; Kim, G. H.; Chang, H. W.; Lee, S. Y. Synthesis and analysis of Ag-doped ZnO. *J. Appl. Phys.* **2006**, *100*, No. 093701.
- (29) Hernández, S.; Hidalgo, D.; Sacco, A.; Chiodoni, A.; Lamberti, A.; Cauda, V.; Tresso, E.; Saracco, G. Comparison of photocatalytic and transport properties of TiO₂ and ZnO nanostructures for solar-driven water splitting. *Phys. Chem. Chem. Phys.* **2015**, *17*, 7775–7786.
- (30) Min, Y.; Zhang, K.; Chen, L.; Chen, Y.; Zhang, Y. Ionic liquid assisting synthesis of ZnO/graphene heterostructure photocatalysts with tunable photoresponse properties. *Diamond Relat. Mater.* **2012**, *26*, 32–38.
- (31) Xu, T.; Zhang, L.; Cheng, H.; Zhu, Y. Significantly enhanced photocatalytic performance of ZnO via graphene hybridization and the mechanism study. *Appl. Catal., B* **2011**, *101*, 382–387.
- (32) Akhavan, O. Graphene Nanomesh by ZnO Nanorod Photocatalysts. *ACS Nano* **2010**, *4*, 4174–4180.
- (33) Wang, J.; Gao, Z.; Li, Z.; Wang, B.; Yan, Y.; Liu, Q.; Mann, T.; Zhang, M.; Jiang, Z. Green synthesis of graphene nanosheets/ZnO composites and electrochemical properties. *J. Solid State Chem.* **2011**, *184*, 1421–1427.
- (34) Meyer, B.; Marx, D.; Dulub, O.; Diebold, U.; Kunat, M.; Langenberg, D.; Wöll, C. Partial Dissociation of Water Leads to Stable Superstructures on the Surface of Zinc Oxide. *Angew. Chem., Int. Ed.* **2004**, *43*, 6642–6645.
- (35) Tocci, G.; Michaelides, A. Solvent-Induced Proton Hopping at a Water–Oxide Interface. *J. Phys. Chem. Lett.* **2014**, *5*, 474–480.
- (36) Quaranta, V.; Behler, J.; Hellström, M. Structure and Dynamics of the Liquid–Water/Zinc-Oxide Interface from Machine Learning Potential Simulations. *J. Phys. Chem. C* **2019**, *123*, 1293–1304.
- (37) Quaranta, V.; Hellström, M.; Behler, J. Proton-Transfer Mechanisms at the Water–ZnO Interface: The Role of Presolvation. *J. Phys. Chem. Lett.* **2017**, *8*, 1476–1483.
- (38) Raymond, D.; van Duin, A. C.; Goddard, W. A.; Hermansson, K.; Spångberg, D. Hydroxylation Structure and Proton Transfer Reactivity at the Zinc Oxide-Water Interface. *J. Phys. Chem. C* **2011**, *115*, 8573–8579.
- (39) Perera, D. C.; Rasaiah, J. C. Exchange Functionals and Basis Sets for Density Functional Theory Studies of Water Splitting on Selected ZnO Nanocluster Catalysts. *ACS Omega* **2022**, *7*, 12556–12569.
- (40) Huang, L.; Gubbins, K. E. Ammonia Dissociation on Graphene Oxide: An Ab Initio Density Functional Theory Calculation. *Z. Phys. Chem.* **2015**, *229*, 1211–1223.
- (41) Tang, S.; Cao, Z. Adsorption of nitrogen oxides on graphene and graphene oxides: Insights from density functional calculations. *J. Chem. Phys.* **2011**, *134*, No. 044710.
- (42) Cai, W.; Piner, R. D.; Stadermann, F. J.; Park, S.; Shaibat, M. A.; Ishii, Y.; Yang, D.; Velamakanni, A.; An, S. J.; Stoller, M.; An, J.; Chen, D.; Ruoff, R. S. Synthesis and Solid-State NMR Structural Characterization of 13C-Labeled Graphite Oxide. *Science* **2008**, *321*, 1815–1817.
- (43) <http://www.chemistry4.me/Gaussian/G09W/help/pbctut2.htm>.
- (44) Sosa, C.; Andzelm, J.; Elkin, B. C.; Wimmer, E.; Dobbs, K. D.; Dixon, D. A. A local density functional study of the structure and vibrational frequencies of molecular transition-metal compounds. *J. Phys. Chem.* **1992**, *96*, 6630–6636.
- (45) Godbout, N.; Salahub, D. R.; Andzelm, J.; Wimmer, E. Optimization of Gaussian-type basis sets for local spin density functional calculations. Part I. Boron through neon, optimization technique and validation. *Can. J. Chem.* **1992**, *70*, 560–571.
- (46) Frisch, M. J. et al. *Gaussian16 Revision C.01*; Gaussian Inc.: Wallingford CT, 2016.
- (47) Dennington, R.; Keith, T. A.; Millam, J. M. *GaussView Version 6*; Semichem Inc.: Shawnee Mission KS; 2019.
- (48) Fukui, K. The path of chemical reactions - the IRC approach. *Acc. Chem. Res.* **1981**, *14*, 363–368.
- (49) Petrik, N. G.; Baer, M. D.; Mundy, C. J.; Kimmel, G. A. Mixed Molecular and Dissociative Water Adsorption on Hydroxylated TiO₂(110): An Infrared Spectroscopy and Ab Initio Molecular Dynamics Study. *J. Phys. Chem. C* **2022**, *126*, 21616–21627.